A Novel K-Distribution Parameters Development System and its Application to MAS/Success Channels

By
Charles J. Drummond and Graeme L. Stephens

Department of Atmospheric Science
Colorado State University
Fort Collins, Colorado

Research was sponsored by NASA Earth System Fellowship grant #NGT5-50007. Additional support was provided under NASA Research grants #NAG5-6637 and #NAG5-2692.

Colorado State University

Department of Atmospheric Science

Paper No. 645

A NOVEL K-DISTRIBUTION PARAMETERS DEVELOPMENT SYSTEM AND ITS APPLICATION TO MAS/SUCCESS CHANNELS

Charles J. Drummond and Graeme L. Stephens

Research Sponsored by NASA Earth System Fellowship Grant #NGT5-50007. Additional support provided under NASA Research Grants #NAG5-6637 and #NAG5-2692.

A NOVEL K-DISTRIBUTION PARAMETERS DEVELOPMENT SYSTEM AND ITS APPLICATION TO MAS/SUCCESS CHANNELS

Charles J. Drummond and Graeme L. Stephens

Research Sponsored by NASA Earth System Fellowship Grant #NGT5-50007. Additional support provided under NASA Research Grants #NAG5-6637 and #NAG5-2692.

A NOVEL K-DISTRIBUTION PARAMETERS DEVELOPMENT SYSTEM AND ITS APPLICATION TO MAS/SUCCESS CHANNELS

Charles J. Drummond and Graeme L. Stephens

Research Sponsored by NASA Earth System Science Fellowship grant #NGT5-50007.
Additional support provided under NASA Research Grants #NAG5-6637 and #NAG5-2692.

Department of Atmospheric Science
Colorado State University
Fort Collins, Colorado 80523

January 1998

Atmospheric Science Paper No. 645

ABSTRACT

A NOVEL K-DISTRIBUTION PARAMETERS DEVELOPMENT SYSTEM AND ITS APPLICATION TO MAS/SUCCESS CHANNELS

A principal component of the modeling of radiative transfer processes in inhomogeneous absorbing-scattering atmospheres is the accurate description of the effects of gaseous absorption. While several approaches to the characterization of gaseous absorption exist, they are invariably limited in their applicability. In this study, the development of a novel approach to the creation of k-Distribution parameters that retain significant spectral information is discussed. The results of an investigation seeking to develop parameters for the 50 channels of the MODIS Airborne Simulator (MAS) instrument as configured during the SUCCESS field experiment, which serve as a preliminary step in the creation of a remote-sensing 'Observing System' for the retrieval of upper tropospheric cloud and water vapor properties are presented. It was found that the approach developed here permits the creation of computationally efficient and remarkably accurate gaseous absorption and related band parameters, which for most of channels considered, produce modeling errors smaller than those likely to be encountered in the instrument measurements themselves. Insights into the relative importance of the sources of observed errors are used to develop an additional, and hitherto unconsidered, constraint which may lead to further improvements in the fidelity of the results obtained from parameters created using the approach developed in this study.

ACKNOWLEDGEMENTS

We thank Dr. Philip Gabriel for his evaluation of this paper. We are also grateful to Dr. Si-Chee Tsay for travel support during the Summer of 1997, and to Dr. Michael King for the use of computer systems at Goddard Space Flight Center. The insights of Professor K. Franklin Evans leading to the novel approach to k-Distribution parameters developed in this study, and his helpfully critical assesments of the procedures used to validate the parameters are also gratefully acknowledged.

This work was sponsored by the NASA/MTPE Earth System Science Fellowship Program, under grant #NGT5-50007. Additional financial support for this research was provided under NASA Research Grants #NAG5-6637 and #NAG5-2692.

Contents

List of Figures

List of Tables

Chapter 1

Introduction

An accurate and computationally efficient description of the effects of gaseous absorption on band radiative transfer within the atmosphere is an important component of forward modeling. Historically, approaches which can be put into three broad categories have been used to accomplish this task. Line-by-line (LBL) modeling, which integrates radiative transfer results over relatively narrow spectral intervals in order to produce band results is the most accurate and least computationally efficient approach. While rigorously valid to the limit of our knowledge of absorption processes, in retrieval schemes requiring many iterations to acheive a convergence to a final solution, or other operational schemes, including General Circulation Models (GCMs), the enormous computational effort required to produce line-by-line results preclude their use. A host of so-called 'Band Models' exist, which seek to replace the details of absorption processes within a band with a set parameters allowing results to be produced from a single calculation. While band models are the most computationally efficient approach to this problem, their results can suffer from gross inaccuracies in description of gaseous absorption, and in all but the most ideal cases, fail to allow an accurate description of often equally important scattering processes. A third approach, broadly categorized as the 'Correlated k-Distribution' (CKD) method, formally defined as the inverse of the Laplace transform of absorption characteristics from spectral space to cumulative frequency distribution space, permits great computational efficiency, and when properly implemented, high fidelity to LBL results.

Conventional CKD approaches have demonstrated great utility in the modeling of band radiative transfer. In models where each wave space interval within a band is of

equal importance to the end result, for example as applied in the radiation schemes in GCMs, such approaches, when appropriately defined, are sufficient to describe accurately the effects of gaseous absorption. However, the loss of spectral space information which accompanies the creation and use of conventional CKD models is a limiting factor that can adversely affect the results obtained when they are used to model measurements made by remote sensing instruments, where the importance of individual wave space intervals varies with instrument sensitivity. Further, in bands where several molecular species contribute to absorption processes, the approach commonly taken to describe such so-called overlapping absorption involves a physically non-sensical implementation of the transmission equivalence concept, in that the mixing of absorption properties from spectrally distinct regions invariably occurs.

It is the long-term goal of this investigator to develop a retrieval scheme which seeks to determine upper tropospheric cloud and water vapor properties from measurements acquired by the Moderate Resolution Imaging Spectroradiometer (MODIS) instrument, scheduled for launch aboard the EOS AM-1 platform in 1998. This retrieval scheme, following the optimal-estimator algorithim philosphy first articulated by Rodgers [26], will involve the determination of a set of MODIS channels from which an 'Observing System' containing relevant electromagnetic information may be constructed. In the interim before MODIS data becomes available, it was planned to develop a preliminary retrieval using data collected by the MODIS Airborne Simulator (MAS) instrument during the SUCCESS field experiment, conducted during the spring of 1996. The MAS instrument, which flies aboard NASA ER-2 aircraft at a height of 20 km, is a 50 channel cross-track scanning radiometer that acquires high spatial resolution imagery of cloud and surface features across an 85.92^o total field of view along the aircraft flight track. The spectral range of the 50 channels, as shown in Figure 1.1, encompass much of the visible and infra-red spectrum. Radiance measurements acquired by this instrument have the potential to provide a wealth information associated with the electromagnetic radiation in each band. Unfortunately, it was found that there were few parameterizations of gaseous absorption in the channels associated with this instrument, and thus a need for such information emerged as a necessary prerequisite to any retrieval development work.

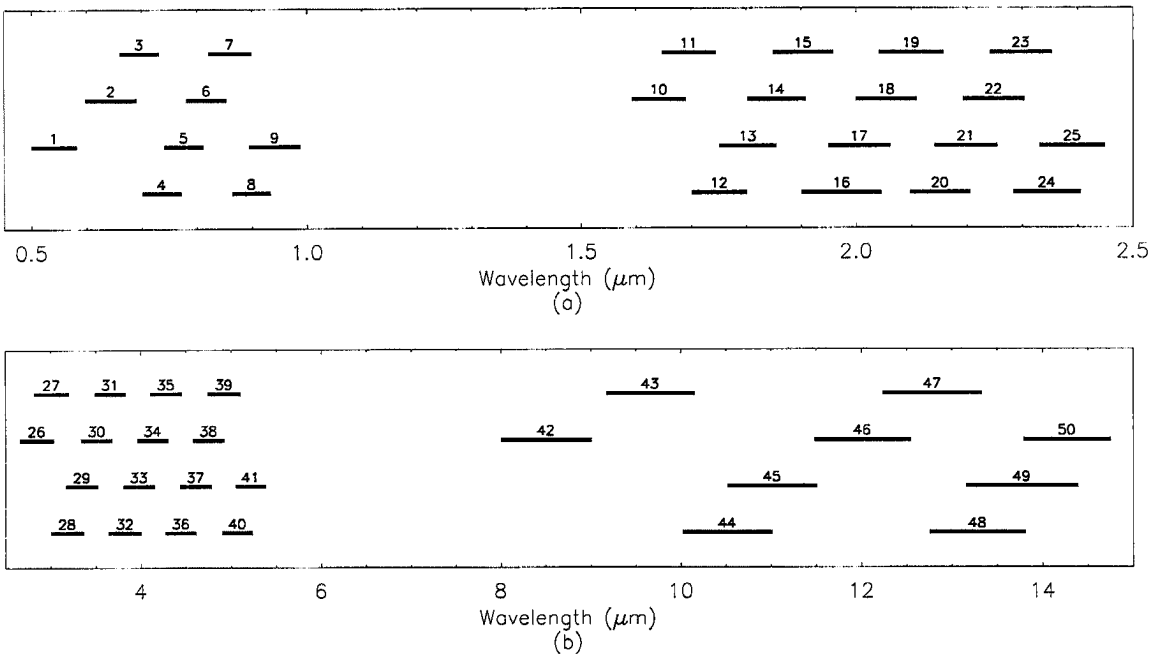

Figure 1.1: MAS/SUCCESS Channel Spectral Extent Definitions. Band extents are determined from calibration Instrument Spectral Response (ISR) functions determined after the SUCCESS field experiment. (a) Band Definitions for Shortwave Ports 1 and 2, (b) Band Definitions for Longwave Ports 3 and 4.

In this study, a novel approach to the creation of Correlated-k distribution parameters for the MAS instrument was developed. Via an extension of the approach to the conventional implementation of CKD parameters, in which the wave-space intervals composing k-distributions are accounted for, some of the spectral information lost in conventional approaches is retained, and overlapping absorption is treated in a way that eliminates much of the mixing of absorption of coefficient information from disparate spectral regions. This additional information allows the inclusion of ancillary spectral information, such as instrument sensitivities, permitting higher model fidelity to instrument measurements.

It was found, through a validation procedure employing a single representative atmospheric profile where the results obtained with the parameters developed here are compared with those obtained from LBL modeling, that excellent agreement occurs for most the 50 MAS bands. Some disagreement between the results of these two approaches is inevitable, but in many cases it was found that the indicated errors were less than instrument's ability

to resolve radiant intensity, and in all but a few cases, less than expected measurement errors associated with the MAS channels.

In the following chapters, the parameters development procedure and results of this investigation are presented. Beginning with a discussion of the nature of atmospheric absorption processes, the creation of synthethic line-by-line absorption spectra from a reference atlas of transition lines is discussed in Chapter 2. The k-distribution approach is introduced in Chapter 3, where a review of other approaches to characterizing band gaseous absorption is also undertaken so as to more firmly define the advantages and limitations of each method. In Chapter 4, the details of the system used to create the parameters developed in this study, and an overview of the parameters themselves are presented. A description of the parameters validation procedure, a summary of the results found for the 50 sets of parameters that were created and a discussion of the sources of the and relative importance of the errors inherent to the parameters is presented in Chapter 5. Finally, a summary of the lessons learned in this study and how they might influence subsequent parameters development efforts is discussed in Chapter 6.

Chapter 2

Creation of Synthetic Absorption Coefficient Spectra

The first step in the development of Correlated k-distribution parameters is the creation of synthetic absorption coefficient spectra, or k-spectra from line transition strength and broadening profile data. These band spectra are created by superposing the Voigt profile broadening contributions from relevant individual transition lines, and is a relatively straightforward, though computationally intensive, process. An overview of the nature of atmospheric absorption processes, while perhaps not the central purpose of this paper, is relevant in so far as understanding the factors that give rise to the differences between k-spectra at different depths in the atmosphere, and as such is discussed at the qualitative level in the following sections.

Before the creation of k-spectra can proceed, the band itself must be defined and the species producing non-negligible absorption within it must be identified. Band extants for the MAS channels were determined from calibration Instrument Spectral Response (ISR) functions developed at NASA/Ames and released late in the Spring of 1997. These ISRs are based on MAS as configured during the SUCCESS field experiment, which took place in April and May, 1996. The 1996 edition of the HITRAN molecular spectroscopic database (Rothman, *et al*, [27], [28]) is the source of line transition strength and broadening data. For each molecular species identified within a band, a set of 78 high-resolution k-spectra, are produced using these HITRAN data and the Voigt line broadening profile, at each of 3 reference temperatures (210 K, 250 K, and 290 K) and each of 26 reference pressures between 0.01 mb and 1000 mb. The k-spectra generation phase of the parameters development is the most computationally intensive portion of creating k-distribution

absorption parameters. During the system's development, which coincided with the generation of the k-spectra for the MAS bands, several optimizations to this part of the process, designed to expedite the spectra generation, were considered. A method which reduced the total computational effort required to produce the k-spectra for the 50 MAS channels by about 43% was finally settled upon. This optimization is discussed along with other potential approaches in more detail below. Even with this optimization method in place, nearly $2 times 10^{12}$ Voigt profile calculations were required and thus some automation of this process was required to finish this phase in a timely manner. An overview of this automation process, as implemented on a multi-processor UNIX workstation is also discussed.

2.1 A Brief Review of The Nature of Atmospheric Absorption

The description of absorption by gaseous constituents in the earth's atmosphere is a rich and complex subject. It is *far* beyond the scope of this paper to cover the phenomena involved thoroughly, but an at least rudimentary discussion of the physics of absorption proceses will serve to provide a foundation from which the development discussed in later chapters may be justified.

The quantization of molecular energy states is at the heart of the model of absorption employed here. A simple (though incomplete) explanation for one type of this phenomea is the concept of the atom as an harmonic oscillator with a set of discrete allowed states (or frequencies) of oscillation. According to Planck's relation, $\Delta E = h\nu$, where h is Planck's constant, the transition from one state to another is accompanied by the emission or absorption of a photon with frequency, ν, proportional to the energy lost or gained between states. Energetic interactions with the environment that effect state transitions can be broken into several categories, each with their own range of accompanying energies as shown in Table 2.1. State transitions can involve more than one transition type, so that for example, a change in electronic state may be accompanied by changes in vibrational, rotational and spin quantum states. Considering the energies involved in the spectrum

Transition Type	Characteristic ΔE
Electronic	a few 10^4 cm^{-1}
Vibrational	500 - 1000 cm^{-1}
Translational	several 10^2 cm^{-1}
Rotational	1 - 100 cm^{-1}
Nuclear spin	negligible

Table 2.1: Characteristic Molecular Transition Energies, in order of decreasing transition energy.

of MAS channels, from the visible to far-infrared, combinations of changes in vibrational and rotational states give rise to many of the absorption bands seen, in that vibrational transitions are usually accompanied by *many* relatively weaker rotational energy transitions.

First considering absorption at the molecular level, the quantum mechanical Hamiltonian operator, H, applied to Schroedinger's wave equation, ψ, can be used to express a system's energetics as

$$\frac{ih}{2\pi}\frac{\partial\psi(x,t)}{\partial t} = H\psi(x,t) \tag{2.1}$$

Separation of variables may be performed, so that the operator may be expressed as a combination of time-independent and time-dependent components as

$$H = H_1(x) + H_2(x,t) \tag{2.2}$$

The time-independent, or *stationary state* component of the Hamiltonian, $H_1(x)$, is further seperable into potential and kinetic energy operators, such that $H = T + V$. Separation of these operators into vibrational and rotational components is possible for the potential energy operator component, which depends only on inter-nuclear separations, but can be complicated and unresolvable for the kinetic energy operator component due to the coupling of the effects of the noninertial reference frame within which molecules may rotate. Provided the time-dependent components of the Hamiltonian operator, $H_2(x,t)$ are small, they may be treated as perturbations to the time-independent component of (2.2). The stationary states have solutions of the form

$$H_1\psi(x) = E\psi(x) \tag{2.3}$$

where $\psi(x)$ are eigenfunctions with discrete eigenvalues, E. When (2.3) is also seperable into the different types of molecular energy, corresponding to the transition types in Table 1.1, the total energy is the sum of the individual energies, and the resultant wave functions are the product of the individual wave functions. The separate components of molecular energy are each specified by quantum numbers, and the complete system is described uniquely by the vector of the individual components. When different combinations of these quantum numbers produce the same total energy state, the energy states are said to be degenerate. The existence and degree of degeneracy is dependent on molecular configuration.

A simplified, non-coupled Hamiltonian, called the *harmonic-oscillator, rigid rotator model*, which is strictly valid for diatomic molecules, has been extended to include up to fourth-order perturbation expansion (interaction) terms for the purpose of describing the variety of molecules present in the terrestrial atmosphere. These perturbation terms account for the effects of centripetal acceleration on vibrational transitions and the corresponding changes in bond length that affect angular momenta. This model has been widely applied in numerical form to describe vibrational, rotational and combined vibrational-rotational transitions.

Time dependent terms in (2.2), which are representative of state transitions, arise from two distinctly different types of processes: from collisional molecular interactions, which serve to change molecular momenta, and from interactions between molecules and ambient electromagnetic fields, which cause changes in molecular dipole moments. The first type of interaction influences the shape of absorption lines, while the second influences line strength (Goody and Yung, [12]).

2.1.1 Translational state transitions and Local Thermodynamic Equilibrium

In the terrestrial atmosphere, state transitions arising from collisions are almost (but, importantly, not completely) instantaneous, since the time between collisions is relatively large compared to the time involved in collisions themselves. Unlike quantum mechanical models of motion in idealized closed systems, the changes in molecular energetics which

accompany collisions in the practically unbounded free atmosphere, while also strictly quantized transitions, do not have stationary states. The translational energy changes that accompany collisions are involved in establishing equilibrium populations of energy levels via Maxwell's distribution of molecular velocities. Maxwell's distribution serves to define the macroscopic kinetic temperature and, when obeyed, the condition of thermodynamic equilibrium.

Atmospheric molecular systems are not generally in a state of complete equilibrium, which is applicable only to idealized closed systems. Rather, the condition of Local Thermodynamic Equilibrium (LTE) of energy state populations, as applied to specific pairs of energy levels is considered instead. Needed to adequately describe emission processes via the Planck function, in the larger scope of radiative transfer in general, translational LTE at a given temperature occurs when the collisional adjustment rate, or *relaxation time*, of state populations, is much less than some molecular constant. In the terrestrial atmosphere, this occurs below an atmospheric level above which molecules may diffuse into and escape through to space without undergoing further collisions. LTE at a given temperature thus serves as a condition under which the Boltzmann factor is a valid means to describe the relative populations between certain groups of levels. The energetics of the terrestrial atmosphere, as observed in MAS bands, involve interactions between vibrational, rotational, and translational states. Goody and Yung [12] show that the condition of disequilibrium between vibrational states, common in the atmosphere, while LTE is observed for rotational and translational states allows for the adequate description of source terms, and thus permits the strictly valid use of the Planck source function up to the lower boundary of the *exosphere*, near 50 km. Above this level, the most important single absorbtion band, the 15 μm CO_2 band, with a radiative lifetime of 0.74s, extends the applicability of the Planck function to near 75km. Above this level, heating rates that may derived with alternative expressions for emission trend toward zero with increasing height and atmospheric transparency, and while essentially invalid above this level, errors resulting from the implicit assumption of LTE are of negligible importance to radiative transfer modeling of the atmosphere as a whole.

2.1.2 Vibrational State Transitions

Interactions with ambient electromagnetic fields that influence absorption line behavior arise primarily from the presence of permanent or vibrationally induced molecular electric dipole moments, which are expressed in matrix form as $\mathbf{M}(\mathbf{q})$, where $\mathbf{q}$ is a vector representing the molecular orientation with respect to the ambient field. Magnetic dipole moments[1] and electric quadrupole moments also play a role, but to a negligible degree as far as atmospheric absorption is concerned. Dipole moment interactions give rise to the strongest absorption bands in the atmosphere, for example the 13.5 μm CO_2 band, which arises from induced, degenerate ν_2 bending vibrational modes of this linear molecule which has no permanent dipole moment. Electric dipole moment transitions are enitrely dependent on molecular configuration, in that the field must act with some component parallel to the dipole orientation, *and* the dipole configuration must change over the course of the transition. The probability of a dipole transition between two quantum states, i, and j, is expressed via the *weighted transition moment squared* as

$$R_{ij} = \int \psi_i^* \mathbf{M} \psi_j \, dV \tag{2.4}$$

where dV is a volume element in configuration space. Since the wave functions, ψ, are by definition orthogonal, if $\mathbf{M}$ is not configuration dependent, it may be taken outside of the integral and (2.4) is zero. Further, (2.4) is also zero for certain combinations of i and j. The particular combinations of states producing nonzero outcomes are termed *selection rules*, and as such are highly dependent on system symmetry.

2.2 Spectral Transition Lines

Having considered the factors that give rise to absorption spectra, it remains to determine the explicit form of transition line strengths, from which k-spectra may be created. The HITRAN database (Rothman, *et al* [27, 28]) contains an atlas of transition lines, their measured intensities at a reference temperature of 296K, and empirically or theoretically

---

[1]The O_2 A-band, centered near 0.76 μm arises from magnetic dipole moment transitions.

derived data to describe the variations in intensities and broadening characteristics with temperature and pressure. From the preceding discussion, it follows that the strength of a transition line is directly dependent on the ability of a population of molecules to undergo energetic transitions associated with photons of a discrete wavelength. Under the condition of thermodynamic equilibrium, the number of molecules per unit volume, N_η in the possibly degenerate quantum states, η, at temperature T is given by the Maxwell-Boltzmann distribution law,

$$N_\eta = N d_\eta \frac{e^{-E_\eta/kT}}{Q(T)} \tag{2.5}$$

where N is the total number of molecules per unit volume, d_η is the total degeneracy of the states η, with energy E_η, the exponential term is the *Boltzmann factor* and $Q(T)$ is the *partition function* defined as the sum of the Boltzmann factor over all physically realizable states, as

$$Q(T) = \sum_i e^{-E_i/kT} \tag{2.6}$$

The fundamental assumption of statistical mechanics is that for a closed system, all accessible quantum states are equally likely. (Kittel and Kroemer [15]). A corollary of the 3rd law of thermodynamics indicates that as the energy of the system increases, the total number of states accessible to the system will increase. Thus the probability of finding members of the system in states susceptible to transitions characterized by photons of a particular energy typically decreases with increasing temperature.

A notable exception to this rule is the existance of so-called "Hot Bands" where the strengths of observed transition lines actually increase with system energy. The majority of lines with appreciable strengths originate from transitions from the ν=0 vibrational ground state to some higher state. According to Banwell [3], in cases where the ν=1 vibrational state has a particularly low frequency, its population may, under certain conditions, become appreciable with respect to all possible states. In such cases, e.g. the $15\mu m$ CO_2 band, the susceptibility of transitions from the ν=1 state will actually increase with temperature over the range in which the ν=1 state becomes increasingly populated.

The Boltzman factor is perhaps best described by considering an idealized case of a set of molecules in some volume element, $\mathcal{S}$, in thermal equilibrium with a much larger

reservoir, $\mathcal{R}$, such that $\mathcal{R}$ and $\mathcal{S}$ together form a closed system. Letting the fixed total energy of this combined system, $\mathcal{R}+\mathcal{S}$, equal U_0, the total number of states accessible to the combined system is the product of the number of the states accessible to $\mathcal{R}$ and $\mathcal{S}$ individually. Considering $\mathcal{S}$ to be in the completely specified, and thus non-degenerate, state s with energy E_s, it follows that the energy of the reservoir is $U_0 - E_s$ and the number of states accessible to the combined system is reduced to the number of acccessible states, or multiplicity, of the reservoir, $g_{\mathcal{R}}(U_0 - E_s)$. Next considering the ratio of the probability that $\mathcal{S}$ is in quantum state 1 with energy E_1 to the probability that $\mathcal{S}$ is in quantum state 2 with energy E_2, it follows that this is also the ratio of the two reservoir multiplicities, so that

$$\frac{P_r(E_1)}{P_r(E_2)} = \frac{g_{\mathcal{R}}(U_0 - E_1)}{g_{\mathcal{R}}(U_0 - E_2)} \tag{2.7}$$

Given that entropy is defined as the logarithm of the number of states accessible to a system, it more convenient to re-write (2.7) in terms of the ratio of reservoir entropies as

$$\frac{P_r(E_1)}{P_r(E_2)} = \frac{\sigma_{\mathcal{R}}(U_0 - E_1)}{\sigma_{\mathcal{R}}(U_0 - E_2)} = \exp\left[\sigma_{\mathcal{R}}(U_0 - E_1) - \sigma_{\mathcal{R}}(U_0 - E_2)\right] \tag{2.8}$$

Since the energy of the reservoir may be treated as a perturbation to the combined system energy, U_0, in the limit $U_0 >> E_i$, it is appropriate to perform a Taylor expansion about $\sigma_{\mathcal{R}}(U_0)$ at constant volume, V, and N, as

$$\begin{aligned} \sigma_{\mathcal{R}}(U_0 - E) &= \sigma_{\mathcal{R}}(U_0) - E(\partial\sigma_{\mathcal{R}}/\partial U)_{V,N} + \cdots \\ &= \sigma_{\mathcal{R}}(U_0) - E/kT + \cdots \end{aligned} \tag{2.9}$$

where $(\partial\sigma_{\mathcal{R}}/\partial U)_{V,N} \equiv 1/kT$, and k is Boltzmann's constant, defines the temperature of the combined system. Thus the ratio of the probabilities of finding the system in either of a pair of particular states is

$$\frac{P_r(E_1)}{P_r(E_2)} = \frac{\exp(-E_1/kT)}{\exp(-E_2/kT)} = \exp\left[-\frac{E_1 - E_2}{kT}\right] \tag{2.10}$$

from which the Maxwell-Boltzmann distribution of energetic states in (2.5) follows as being proportional to the number of molecules, the quantum energy state degeneracy, and the normalized state probability, $e^{-E_s/kT}/Q(T)$.

To produce k-spectra at the 3 temperatures employed in this study, the reference line intensities in the HITRAN database must be adjusted to account for the changes in occupancies that accompany variations in temperature. From (2.5), it follows that line intensities will scale with the occupancies of states with permitted transitions, such that the product of the transition line intensity and the Maxwell-Boltzman distribution is constant with temperature. Thus, for two temperatures, T_0 and T,

$$S(\eta, T_0)\frac{d_\eta \exp\left[-\frac{hc}{k}\frac{\eta}{T_0}\right]}{Q(T_0)} = S(\eta, T)\frac{d_\eta \exp\left[-\frac{hc}{k}\frac{\eta}{T}\right]}{Q(T)} = Constant \tag{2.11}$$

Given that the absorption spectra observed in the visible through IR bands are the result of combinations of vibrational-rotational transitions, it is useful to consider the partition function in terms of separate vibrational and rotational partion function components for the electronic ground state. Assuming seperability of the vibrational and rotational energies of a molecule,

$$Q(T) = \frac{1}{\sigma}Q_{vib}(T) \times Q_{rot}(T) \tag{2.12}$$

where σ is 2 for homonuclear diatomics and 1 otherwise (Gamache, *et al* [9]), and $Q_{rot}(T)$ considers all of the relatively finely resolved rotational levels in a limited frequency range near the purely vibrational energy state, such that $\nu/\nu_0 \sim 1$, and

$$\begin{aligned} Q_{rot}(T) &= \sum_i \exp\left[-\frac{E_{rot,i}}{kT}\right] \\ &= \sum_i \exp\left[-\frac{hc|\nu_i - \nu_0|}{kT}\right] \\ &= d_{rot}\frac{1}{1-\exp\left[-\frac{hc}{k}\frac{\nu_0}{T}\right]} \\ &= d_{rot} \times Q'_{rot}(T) \end{aligned} \tag{2.13}$$

where hc/k=1.438786 cm·K is defined in terms that convert the energies involved to cm^{-1}, and d_{rot} is rotational degeneracy which is a molecularly dependent quantity that may also depend on the particular vibrational mode having energy ν_0.

The HITRAN database includes data and code to calculate the so-called *Total Internal Partion* (TIP) function for a given molecule, isotopic variant and temperature in the range 70 K to 3000 K, according to a cubic polynomial. This quantity, $Q_{tot}(T)$, is used

in conjuction with the temperature dependent rotational partion function component to adjust line intensities to arbitrary temperatures. The line strength, $S(\nu_0)$ at arbritrary temperature T, within the wide range of validity of $Q_{tot}(T)$ is then found in terms of the line strength at the reference temperature, T_0=296K, as

$$\begin{aligned} S(\nu_0,T) &= S(\nu_0,T_0)\frac{Q_{tot}(T_0)Q'_{rot}(T_0)}{d_{E_l}\exp\left[-\frac{hc}{k}\frac{E_l}{T_0}\right]} \Big/ \frac{Q_{tot}(T)Q'_{rot}(T)}{d_{E_l}\exp\left[-\frac{hc}{k}\frac{E_l}{T}\right]} \\ &= S(\nu_0,T_0)\frac{Q_{tot}(T_0)}{Q_{tot}(T)}\frac{Q'_{rot}(T_0)}{Q'_{rot}(T)}\exp\left[\frac{hc}{k}E_l\frac{(T-T_0)}{TT_0}\right] \\ &= S(\nu_0,T_0)\frac{Q_{tot}(T_0)}{Q_{tot}(T)}\frac{1-\exp\left[-\frac{hc}{k}\frac{\nu_0}{T}\right]}{1-\exp\left[-\frac{hc}{k}\frac{\nu_0}{T_0}\right]}\exp\left[\frac{hc}{k}E_l\frac{(T-T_0)}{TT_0}\right] \end{aligned} \tag{2.14}$$

where $S(\nu_0,T_0)$ is the reference line strength at ν_0 and E_l is the lower state energy, in cm^{-1}, from which molecules may be excited by absorbing a photon with energy ν_0.

2.3 Line Identification

After defining the band begining and ending wavenumbers, the molecular species with relevant state transitions must be identified. Absorption coefficient spectra generation for all of the absorbers 'active' in the MAS bands coincided with other aspects of the systems development, and as such, relevant absorber identification has been refined along the way.

At the time of initially identifying the species to include in a MAS band, a rather simplistic approach was taken, in that all of the species with *any* transition lines were identified and an *ad hoc* (albeit conservative) guess as to their relevance made. As a refinement to this approach, relatively low-resolution k-spectra were created for a state representative of a homogeneous atmosphere with a pressure of 500 mb, temperature of 250 K at 1 cm^{-1} interval resolution for each of the species with transition lines within a band, and column transmissions, using 1976 U.S. Standard Atmosphere optical paths, determined. As a result of this screening process, only those species with non-negligible band column transmissions (by default less than 0.9999) were selected for further use.

The fundamental form of the monochromatic optical depth contribution, at wavenumber ν, due to a spectrally broadened transition line centered at the wavenumber ν_0 for the

ith isotope of a molecule, through an optical path, u, at pressure p and temperature T, is given by

$$\tau_\nu(\nu_0, p, T, u) = S'(\nu_0, T) f(\nu - \nu_0, p, T) A_i u \tag{2.15}$$

where $S'(\nu_0, T)$ is the transition line intensity, $f(\nu - \nu_0, p, T)$ is the line-broadening profile, and A_i is the (dimensionless) relative abundance of the ith isotope. Relative isoptopic abundances are incorporated into the reference transition line strength values, $S(\nu_0, T_0)$, i.e., $S(\nu_0, T_0) = S'(\nu_0, T_0) A_i$. Synthetic k-spectra, k_ν, at a particular reference temperature and pressure are generated by superposing the contributions from all transition lines such that the monochromatic optical depth at wavenumber ν due to N relevant lines is given by

$$\tau_\nu(p, T, u) = \sum_{j=1}^{N} S_{\nu_0(j)}(T)\ f(\nu - \nu_0(j), p, T) u = k_\nu(p, T)\ u \tag{2.16}$$

2.4 Use of the Voigt Profile

In the lower atmosphere, radiative transitions are disturbed by molecular collisions and thus spectral transition lines are broadened over some spectral width. This pressure broadening is characterized by the Lorentz profile as a function of pressure and temperature and follows from the solution to Schroedinger's wave equation (Goody and Yung, [12]) as

$$f_L[(\nu - \nu_0), p, T) = \frac{\alpha_L(p, T)}{\pi\left[(\nu - \nu_0)^2 + \alpha_L(p, T)^2\right]} \tag{2.17}$$

where α_L is the spectral distance from line center to where the measured absorption falls to one-half of its maximum, and is referred to as the *line width.* The line width scales with pressure and temperature in terms of reference conditions, (p_0, T_0) as

$$\alpha_L(p, T) = \alpha_{L_0} \left(\frac{p}{p_0}\right) \left(\frac{T_0}{T}\right)^n \tag{2.18}$$

where n is molecularly dependent, and $\alpha_{L_0} = 1/(2\pi\tau)$ is the reference line width, at which τ is the mean residence time of excited states resulting from *optical collisions.* The term *optical collisions* is broader in scope than that used to define *kinetic collisions* as considered above, in that collisions producing any state transition (i.e. including rotational

transitions as opposed to just momentum transitions) are considered. Directly proportional to pressure, the widths of lines are dissimilarly affected by collisions between like molecules (self-broadening) and unlike molecules (foreign-broadening), due to exact resonance effects which are more likely to occur in collisions between like molecules. Since the radiatively active absorbers considered in this study occur in relatively low concentrations, only foreign-broadening is considered. Line shape departures from the Lorentz profile are known to occur at spectral distances greater than the half-width (Stephens, [30]), but are difficult to measure and thus parameterize. In the absence of any alternatives, the Lorentz profile is assumed valid for any single line across the extant of the band in which it appears.

In the upper atmosphere, where pressure, and thus the frequency of collisions, is relatively low, Lorentz broadening plays only a minor role. However, the molecular velocities associated with relatively high kinetic temperatures become a significant source of broadening along any observational path. In the reference frame of the observer, absorption lines of relatively fast moving molecules are Doppler shifted from their source frequency. Under conditions of thermodynamic equilibrium, molecular velocities will follow the Maxwell distribution, such that the probability of observing an absorption coefficient that is shifted some spectral distance from its origin follows from it. Defining the Doppler line width as

$$\alpha_D = \frac{\nu_0}{c}(2RT)^{1/2} \tag{2.19}$$

where R is individual gas constant, the Doppler profile is derived from the Maxwell velocity distribution as

$$f_D(\nu - \nu_0) = \frac{1}{\sqrt{\pi}\alpha_D} \exp\left[-\frac{(\nu - \nu_0)^2}{\alpha_D^2}\right] \tag{2.20}$$

While the Lorentz and Doppler line profiles are good approximations to broadening in the limits of high and low pressure, respectively, a profile which accurately takes account of both processes is preferred in terms of general applicability.

The Voigt profile, which is formally defined as the convolution of Lorentz and Doppler broadening contributions as

$$f_V(\nu - \nu_0) \quad = \quad \int_{-\infty}^{\infty} f_L(\nu' - \nu_0)\ f_D(\nu - \nu')\ d\nu'$$

$$= \frac{1}{\pi^{3/2}} \frac{\alpha_L}{\alpha_D} \int_{-\infty}^{\infty} \frac{1}{(\nu' - \nu_0)^2 + \alpha_L^2} \times \exp\left[-\frac{(\nu' - \nu_0)^2}{\alpha_D^2}\right] d\nu' \quad (2.21)$$

where

$$\int_{-\infty}^{\infty} f_V(\nu - \nu_0)\, d(\nu - \nu_0) = 1 \quad (2.22)$$

satisfies this pressure independent applicability requirement, in that it combines the separate components leading to observed broadening into a single expression. A closed form approximation to (2.21), required to numerically implement the Voigt profile, developed by Formichev and Shved [7], agrees to within 3% of (2.21) over a wide range of parameters. They find

$$\begin{aligned} f_V(\nu - \nu_0) &= \left(\frac{\ln 2}{\pi}\right)^{1/2} \frac{1}{\alpha_V}(1 - \zeta) \exp(-\ln 2\eta^2) \\ &+ \frac{1}{\pi\alpha_V}\zeta\frac{1}{1+\eta^2} - \frac{1}{\pi\alpha_V}\zeta(1-\zeta)\left(\frac{1.5}{\ln 2} + 1 + \zeta\right) \times \\ &\left(0.066\exp(-0.4\eta^2) - \frac{1}{40 - 5.5\eta^2 + \eta^4}\right) \end{aligned} \quad (2.23)$$

where $\zeta = \alpha_L/\alpha_V$, $\eta = (\nu - \nu_0)/\alpha_V$, and the Voigt line width is

$$\begin{aligned} \alpha_V &= 0.5\left[\alpha_L + (\alpha_L^2 + 4(\ln 2)\alpha_D^2)^{1/2}\right] \\ &+ 0.05\alpha_L\left[1 - \frac{2\alpha_L}{\alpha_L + (\alpha_L^2 + 4(\ln 2)\alpha_D^2)^{1/2}}\right] \end{aligned} \quad (2.24)$$

2.5 Line-by-Line Spectra Generation Procedures

Pulling together the forms of the line strength and broadening profiles described above, k-spectra at a specific temperature and pressure are determined at each of the line-by-line wavenumber intervals, ν_i, by superposing the contributions from each of the N relevant transition lines as

$$k(\nu_i, p, T) = \sum_{j=1}^{N} S_j(\nu_j, T) f_V(\nu_i - \nu_j, p, T) \quad (2.25)$$

In addition to the absorption lines appearing within a band, additional lines from some distance outside of the band are included so that the resultant k-spectra will include their broadened contributions. For a band defined over $[\nu_0,\ \nu_1]$, transition lines within the spectrum $[\nu_0 - \delta\nu,\ \nu_1 + \delta\nu]$, where $\delta\nu = (\nu_1 - \nu_0)/10$ were typically included.

2.5.1 Optimizations to k-Spectra Generation

As indicated in (2.25), the computational effort involved in producing a single k-spectra is proportional to the N lines as well as to the number of wavenumber intervals used to describe the band. In bands with a large number of absorption lines and/or where a great number of wavenumber intervals are required to adequately resolve the details of absorption, significant computational effort is required to produce the k-spectra needed in k-distribution parameters development. In addition to the 78 k-spectra needed to produce the parameters, an additional set of 34 somewhat lower resolution k-spectra for each absorber were also created for use in line-by-line radiative transfer modeling validations. Considering that overlapping absorption by more than one molecular species is typically important in each channel[2], a valid means to optimize the generation process seemed imperative.

Given that the form of the line profile is symmetric about the line center, an optimization which calculates $f_V(\nu - \nu_0)$ once for each spectral distance from a line center, $|\nu - \nu_0|$, was used to reduce the computational effort. It can be shown that for a band with a uniform random distribution of absorption lines only occuring within the band extents, this optimization will reduce the computational effort by ~25%. In the actual MAS spectra, where lines are somewhat less than randomly distributed and the inclusion of wing contributions from outside of the band reduces this optimization's applicability even further, it was found that this optimization alone would reduce computational effort, on average, by ~17.8%.

An additional optimization that was considered early in this study involved truncating the inclusion of line broadening effects at some distance proportional to the Lorentz line width. While this approach had the potential to save significant computational effort, discontinuties in the k-spectra were observed to result from the truncation of stronger lines. Another approach used by some investigators (e.g. Burch [4]) that eliminates these

---

[2]In total, 151 absorber k-spectra sets, each set composed of 78+34=112 k-spectra, were required for the 50 MAS channels.

discontinuities involves the inclusion of an *apodized bound* term to the form of the line profile that varies linearly between 1 and 0 between two spectral distances from line center. While this proceedure removes the discontinuities that result from simple truncation, it lacks a firm physical basis, and situations where significant wing contributions from strong lines would be neglected seemed likely, and was thus not employed. In retrospect, considering the uncertainties about the applicability of the Lorentz profile in far wings, their typically unimportant contribution to total absorption over all but the longest optical paths, and the availibility of other parameterizations to include such *continuum absorption* by water vapor (e.g., Clough, et al, [5], [6]) in window regions, an appropriately conceived apodization scheme may be useful in future applications.

Given the wide range of lines that may found in a band, which can vary in strength by several orders of magnitude, it is not hard to conceive that some of the weaker lines are of negligible consequence to band-averaged optical depths. Since the computational effort required to produce k-spectra is proportional to the number of lines included, the elimination of such lines could serve to expedite k-spectra generation without adversely affecting their fidelity. With this in mind, what turned out to be a significant optimization to k-spectra generation was designed. This approach considers the effect of neglecting lines with strengths less than some cutoff value on the spectrally integrated average absorption coefficient, $\overline{k}$, determined for the band $[\nu_0,\nu_1]$ resolved to $\Delta\nu$ as

$$\overline{k} = \frac{1}{\nu_1 - \nu_0} \sum_i k(\nu_i)\Delta\nu_i \tag{2.26}$$

In this optimization process, all of the transition lines relevant to a band are first identified and counted so that an appropriate line resolution, not less 5 per cm^{-1}, can be used to create test k-spectra relatively quickly, while preserving as many of the spectral details as possible. At each of the 26 standard pressure levels needed for each absorption band, an algorithm which evaluates the effect of neglecting lines with strengths below a reference temperature cutoff value, $S_{cut}(T_0)$, on $\overline{k}$ is then employed. A reference average absorption coefficient $\overline{k}_{ref}$ is first determined after creating a k-spectrum that includes all lines. The median line strength, S_{med}, is then identified, a second k-spectrum which

neglects all lines with $S < S_{med}$ created, and the corresponding $\overline{k}_{med}$ is determined. Based on whether the ratio of $\overline{k}_{med}$ to $\overline{k}_{ref}$, $p_{med} = \overline{k}_{med}/\overline{k}_{ref}$, is greater than or less than a required precision, p_{req}=0.9999 (i.e., whether the neglection changes $\overline{k}$ by less than or more than 0.01%), one of two approaches is then taken. For median cutoff spectra where $p_{med} > p_{req}$, the range between the band's strongest line strength, S_{max}, and S_{med} is split into $\Delta S = (S_{max} - S_{med})/5$ increments and, starting with a cutoff line strength value of $S_{cut} = S_{max} - \Delta S$, the procedure is iterated for each S_{cut} until $p_{cut} < p_{req}$, at which point the previous S_{cut} is retained. A similar approach is employed for reference pressures where $p_{med} \leq p_{req}$. In this case, the minimum line strength, S_{min} is identified and the iterative process begins at $S_{cut} = S_{min} + (S_{med} - S_{min})/5$. The procedure is employed using a reference temperature of 210K, since this temperature typically produces the greatest dynamic range in $k(\nu)$, and early tests using all three reference temperatures indicated that results at 210K required the lowest (i.e., the most conservative) cutoff values. For the line-by-line validation k-spectra, which are generated at layer average pressures falling between reference pressures, the lower of the two S_{cut} values that straddle the specific layer pressure is used.

This optimization is justified by considering how the subtraction of the neglected lines affects the resultant k-spectra. The relative precision criterion ensures that broadening contributions of neglected lines are of negligible consequence to absorption over the band as a whole, but their effect on spectral details near neglected line centers is not directly addressed. During the development of this optimization, in addition to the relative precision tests, visual comparisons of k-spectra created with and without this optimization, and examinations of the specific $k(\nu)$ contributions from neglected lines were performed. In most cases, the neglected line centers appear relatively far below the superposed k-spectra, such that the wing contributions of stronger lines makes the neglected lines difficult to detect at all but extremely highly resolved k-space plots. This suggests that the neglect of such weak details will not have a measureable effect on spectrally resolved radiative transfer. While this optimization approach is computationally intensive in its own right, given that the test k-spectra are created at resolutions that are typically about 3 orders of

magnitude less than those used in other parts of the development process, to the degree that it reduces the total computational effort required, this optimization is a significant development.

The combination of the profile-symmetry and weak-line-neglection optimizations, as employed in this study, produced significant savings in the computational effort required to produce the k-spectra needed for the 50 MAS bands. An examination of the optimization process revealed that a total of 3.260×10^{12} Voigt profile calculations would be required if neither were employed. With the profile-symmetry optimization alone, 2.679×10^{12} calculations would be required, producing an overall savings of 17.81%. With both optimizations in place, 1.851×10^{12} calculations were required, reducing the overall computational effort by 43.23%.

2.5.2 Automation of k-spectra Generation

In total, nearly 12,000 distinct k-spectra were required to produce the complete set required for the parameters development and subsequent validation tests performed in this study. A machine with 4 CPUs and sufficient memory to permit the concurrent generation of separate k-spectra on each CPU being made available, some additional effort to minimize the time required to produce the complete set was made. Several shell scripts that worked in concert with a low-priority scheduling queue, maintained a system load that permitted several spectra to be generated at once, while not seriously compromising the ability of others to use the system. This series of scripts kept track of the status of band-absorber specifc sets of k-spectra, and as jobs were started, freeing up limited queue space, additional sets were submitted for processing. Though some initial operating system problems caused the procedure to break down with the result that submitted jobs disappeared, these problems were eventually overcome through additional tracking procedures that automatically re-submitted jobs gone missing, so that the machine was kept fully occupied creating k-spectra for about one month.

2.6 Summary

The features observed in atmospheric absorption spectra relevant to MAS bands arise from combinations of vibrational, translational, and rotational state transitions. The shape and strength of particular absorption lines are influenced in complementary ways by the effects pressure, temperature, and molecular geometry. Absorption line data, derived from reference parmeters in the HITRAN database, were used to create k-spectra at particular pressure, and temperature combinations for subsequent use in k-distribution parameters development and validation processes via the superposition of broadening contributions from transition lines within and in the vicinity of bands. The MAS channel bands, defined from calibration ISRs, required the generation of nearly 12,000 individual k-spectra, though through the combination of two distinct optimization procedures, the computational effort required was reduced by about 43%.

Chapter 3

The k-Distribution Transform

The k-distribution transform is a means by which the absorption processes relevant to radiative transfer calculations in absorbing-scattering atmospheres can be efficiently and accurately described. While other band approaches to describe absorption processes exist, they are invariably limited in their application. In this chapter, the k-distribution method, formally defined as the inverse of the Laplace transform of k-spectra from wavenumber to cumulative probability distribution space, is initially developed for homogeneous atmospheres with a single active absorber. The advantages of this approach to describe gaseous absorption processes, relative to other methods, is discussed. A review of approaches to its extension to inhomogeneous atmospheres where overlapping absorption by more than one species is important is then undertaken, and the novel approach to overlapping absorption taken in this study is introduced.

Line-by-line methods, which integrate the results of radiative transfer calculations over narrow spectral intervals, are rigorously valid for all types of absorption bands, and serve as the 'truth' against which the results of other methods may be compared. Due to the large number of computations required to model broad-band radiative transfer, especially in spectral regions where k-coefficients change rapidly with wavenumber, their use is impractical in operational or retrieval schemes.

A host of so-called *band models* exist which seek to reduce the distribution of absorption spectra to a set of more tractable parameters. One of the most historically significant of these methods is the van de Hulst, Curtis, Godson (HCG) approximation for inhomogeneous atmospheres, which replaces the line-by-line spectra with pressure and temperature

scaled equivalent mean absorption intensity values. Used in conjuction with absorber path scaling as a function of layer-mean pressures and temperatures, a means to describe absorption over inhomogeneous optical paths is possible. While computationally efficient and valid for weak lines, for strong Lorentz lines and for Doppler lines (Goody, [12]), execptions to its applicability exist, notably in the 9.6 μm O_3 band, where the inverse pressure-concentration distribution of ozone complicates the path scaling method. More generally, problems also arise in spectral regions where absorption is neither strong nor weak. In the context of calculations that include the effects of absorbing and scattering processes, where individual photons may traverse widely varying path lengths, two-parameter scaling methods fail to accurately describe pressure-induced changes in atmospheric absorption.

The Malkmus band model (Malkmus, [21]) also employs two-parameter scaling of line widths and strengths in terms of the band mean absorption line half width, mean absorption line strength, and mean line spacing. The fundamental premise of this approach lies in the validity of the statistics used, in that "randomly distributed, overlapping Lorentz lines with [an] exponentially tailed S^{-1} line-strength distribution" are required. Problems with transmission calculations in bands that do not meet these requirements can be overcome to some degree by fitting model parameters to observed spectra. However, when applied in the context of absorbing-scattering atmospheres, large errors can occur when the full extent of absorption is not accurately described by spectral-mean values. Potentially problematic for absorption by a single species, the Malkmus model is of questionable validity in treating overlapping absorption since the product of two Malkmus bands is not itself a Malkmus band except in the strong- and weak-line limits (Goody, *et al*, [11]). Several other band models exist, and while each may be applicable to specific types of absorption bands, a more generally valid approach is required to expedite radiative transfer calculations that include the effects of gaseous absorption in scattering atmospheres.

3.1 The k-distribution transform in a homogeneous atmosphere

The k-spectra, as developed in Chapter 1, display an essential feature that serves as the basis for the development of the k-distribution method: that the coefficient strengths are

repetitive in the wavenumber-space domain. That is to say, within a band characterised by absorption coefficient spectra occuring between some minimum and maximum values, a given value of k is likely to occur more than once within the band. The k-distribution method exploits this feature to transform from the rapidly varying ordinate in wavenumber space to cumulative probability space, where the abscissa, g, represents the portion of the band where the ordinate, k, is weaker than or equal to $k(g)$. This function is by definition monotonic and turns out to be much smoother than the spectra in wavenumber space. It is thus both more amenable to numerical integration and the assignment of representative k-values over relative wide regions of g-space. This leads to tremendous improvements in computational efficiency relative to the tedious line-by-line approach, while preserving details of absorption that may be lost in band model approaches.

The k-distribution method has been the subject of several studies seeking to improve the characterization of gaseous absorption processes. The method was first proposed by Ambartzumian [2] who used it to estimate the influence of absorption lines on radiative transfer in stellar atmospheres. A single distribution, that was assumed to be representative of the measureable atmosphere, was developed under the hypothesis that the transmittance within a spectral interval is independent of the ordering of the value of k with respect to wavenumber. Rather, it depends only on the fraction of the interval that is associated with a particular value of k. Lacis and Hansen [18] first applied the method to terrestrial atmospheres, employing a single k-distribution along with path scaling to approximate the effects of water vapor absorption in absorbing-scattering atmospheres.

For the purposes of radiative transfer, a "homogeneous" atmosphere is one in which the k-coefficient is constant at a given frequency. For such constant k_ν, integration of absorber density, ρ, over the atmospheric path reduces to $u = \int \rho(z)dz$ and the band averaged transmission over the spectral range $[\nu_0,\ \nu_1]$ is determined by integrating over the band as

$$T(u) = \frac{1}{\nu_1 - \nu_0} \int_{\nu_0}^{\nu_1} \exp(-k_\nu u)\ d\nu \tag{3.1}$$

Equivalently, for line-by-line spectra of sufficiently fine resolution, (3.1) is replaced by the sum over the N wavenumber intervals in the band as

$$T(u) = \frac{1}{\nu_N - \nu_1} \sum_{j=1}^{N} \exp(-k_j u)\ \Delta\nu_j \tag{3.2}$$

where $\Delta\nu_j$ represents the width of the j^{th} line-by-line spectral interval.

The first step toward creating a k-distribution is the regrouping of absorption coefficients into subintervals, or bins, of widths Δk_i. A "frequency distribution" of the line-by-line spectra is thus created by summing the incidence of the wavenumber-space intervals falling into each bin as

$$f(k_i) = \frac{1}{\nu_1 - \nu_0} \sum_{j}^{N} \left| \frac{\Delta\nu_j}{\Delta k_i} \right| W(k_i, k_i + \Delta k_i) \tag{3.3}$$

where $W(k_i, k_i + \Delta k_i)$ is i^{th} bin "window" function equal to unity for wavespace intervals, j, with $k_i < k_j \leq k_i + \Delta k_i$, and zero otherwise. This distribution of line-interval strengths is normalized to unity over the spectral interval $[\nu_0,\ \nu_1]$, and leads to the creation of cumulative distribution increments, $\Delta g_i = f(k_i)\Delta k_i$, which define the fraction of $[\nu_0,\ \nu_1]$ containing absorption coefficients between k_i and $k_i + \Delta k_i$. A depiction of this process is shown in Figure 3.1. Frequency distributions are illustrated in Figures 3.1b and 3.1d, that correspond to the MAS Channel 50 CO_2 k-spectra at 1.0 mb and 1000.0 mb, shown in Figures 3.1a and 3.1c. The rapidly changing nature of the frequency distributions is indicative of relatively large numbers of wavenumber intervals falling within particular frequency bins, and as can be seen directly from the k-spectra plots, coincide well with absorption line centers. The log-log nature of the plot might suggest that line broadening is responsible for much of the absorption process. It should be emphasized, however, that abosorber path-lengths are the determining factor in the attenuation of incident radiation, in that only over relatively long paths will all but the strongest portions of distribution 'actively' contribute to the total absorption.

The non-smooth nature of the frequency distribution makes it inconvenient to use in numerical applications so the more convenient cumulative frequency distribution, defined in continuous and discrete forms respectively as

$$g(k) = \int_0^k f(k)\ dk\ \simeq \sum_{k_i=k_{min}}^{k_i=k} f(k_i)\ \Delta k_i \tag{3.4}$$

where i is the bin number corresponding to those $k_i < k \leq k_i + \Delta k$. Since $g(k)$ is monotonic, it is possible to unambiguously invert it to define the "k-distribution", as

$$k(g) = g^{-1}(k) \tag{3.5}$$

Depicted in Figures 3.1d and 3.1e, the k-distributions corresponding to the k-spectra are devoid of the spikes seen in the frequency distributions and are thus more amenable to the numerical integrations performed when using them in transmission calculations. The k-distribution has been described (Lacis and Oinas [20]) as "a pseudo-absorption line profile that has the same nongray transmission properties ... as the original absorption coefficient spectrum." The normalization over the band employed in (3.3) makes integration over the g-coordinate analogous to integration over the frequency domain. In this light, the band averaged transmission can be determined via integration over the k-distribution. In the case of a singly-absorbing homogeneous atmosphere, the band averaged column transmission is thus determined as

$$T(u) = \int_0^1 \exp\left[-k(g)u\right]\ dg \ \simeq \ \sum_{i=0}^{N} \exp\left[-k(g_i)\right]\ \Delta g_i \tag{3.6}$$

The equivalence shown for the discrete form of (3.6) can be considered exact to the limits of machine precision when numerically implemented with sufficiently resolved bins. In this study bin sizes were chosen in terms of $\log_{10}$ changes in abosrption coefficient strength. This approach, which follows that used by Lacis and Oinas [20], has the advantage of finely resolving Δg intervals in regions where the k-distribution changes rapidly with g. A default resolution of 500 bins per decade strength k was employed when transforming the MAS band spectra, and found to be adequate for most of the bands. Cases where higher resolutions were required are discussed in the next chapter.

3.2 Advantages of the k-distribution Approach

Considering the frequency distribution defined in (3.3) and taking Δk to the infintessimal limit dk, the band averaged transmission can also be written as

$$T(u) = \frac{1}{\nu_1 - \nu_0} \int_0^\infty f(k) \exp(-ku)\ dk \tag{3.7}$$

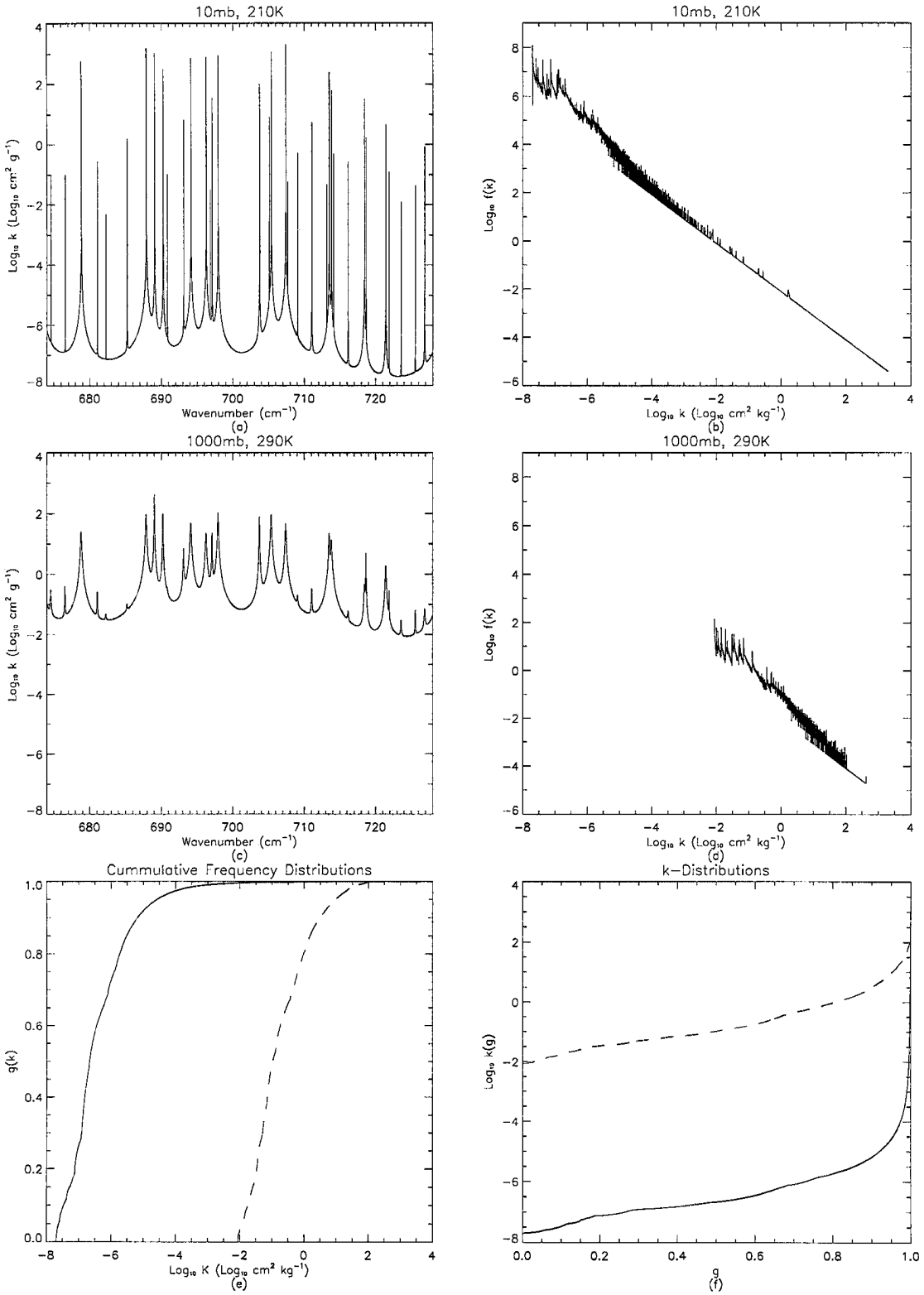

Figure 3.1: Absorption coefficient spectrum for the MAS Channel 50 H_2O band. (a) Line-by-line absorption coefficients (k-spectra) at 10 mbar and 210K and (c) at 1 bar and 290K. (b and d) Absorption coefficient frequency distributions corresponding to k-spectra in Figures 3.1(a) and 3.1(c), respectively. (e) Cumulative frequency distributions of the k-spectra in Figures 3.1(a) (solid) and 3.1(c) (dashed). (f) The k-distributions of the k-spectra in Figures 3.1(a) (solid) and 3.1(c).

This expression defines $f(k)$ as a spectral function that has $T(u)$ as it Laplace transform, i.e., $T(u) = \mathcal{L}[f(k)]$. When continuous and analytic, $\mathcal{L}[f(k)]$ may be inverted to define $f(k)$ as the inverse of the Laplace transform of the transmission function. Goody and Yung [12] discuss this view of the frequency distribution in the larger context of any analytic function of frequency which interacts with the local radiation field. A *major* advantage of the k-distribution over band models emerges when it is considered in this context. Consider, for example, the expression for the thermal emission and scattering source contributions in a medium across some infintessimal path, ds,

$$dI_\nu = e_{v,\nu} J_\nu ds = [k_\nu \rho J_\nu + s_\nu J_\nu]\, ds \tag{3.8}$$

where $e_{v,\nu}$ is the *volume extinction coefficient*, $s_{v,\nu}$ is the *volume scattering coefficient*, and J_ν is a spectrally dependent source function. When angularly dependent scattering is considered, the *scattering phase matrix*, $\mathbf{P}_{ij}$, which describes the propensity for radiation incident at angle ζ_i to be scattered at an angle ζ_j, comes into play, the exitant radiance at angle ζ_e is a function of the integral of contributions of incident radiation over all infintessimal angles $d\omega_s$, i.e.,

$$d\mathbf{I}_\nu(\zeta_e) = s_{v,\nu} ds \int_{\omega_s} \mathbf{P}_{ij}(\zeta_i, \zeta_j) \mathbf{I}^i_\nu(\zeta_i)\, \frac{d\omega_s}{4\pi} \tag{3.9}$$

where $\mathbf{I}^i_\nu(\zeta_i)$ is the incident intensity. The angularly dependent source function, from (3.8) and (3.9), is then

$$\mathbf{J}_\nu(\zeta_e) = \frac{s_{v,\nu}}{e_{v,\nu}} \int_{\omega_s} \mathbf{P}_{ij}(\zeta_i, \zeta_j) \mathbf{I}^i_\nu(\zeta_i)\, \frac{d\omega_s}{4\pi} \tag{3.10}$$

indicating a spectrally dependent coupling between sources and the absorption coefficients. Band-model approaches, which replace spectral quantities by band-averaged quantities, implicity assume that such scattering source functions can be adequately determined from mean transmissions. The form of (3.10) indicates that this assumption is easily invalidated, since for any spectral interval in which absorption properties and/or incident radiation vary significantly with ν, the band-averaged mean of (3.10) *will not* be adequately approximated by the mean-values employed. This essential limitation precludes the use of band models in radiative transfer calculations that include scattering over arbitrary bands, and points to an inherent superiority of k-distribution approaches when such spectral variability is adequately approximated by appropriately defined Δg intervals.

3.3 Extension to Nonhomogeneous Atmospheres

Though obviously problematic in scattering atmospheres, band-models, when valid in purely-absorbing atmospheres are able, via scaling parameters, to resolve the effects of pressure and temperature inhomogeneities on line-broadening behavior. The wavenumber-space scrambling that accompanies the creation of conventional k-distributions directly from k-spectra destroys the k-spectra's relationship to absorption lines and, at first glance, would seem to require the recalculation of k-distributions for each combination of pressure and temperature of interest. One way of overcoming this limitation is to create k-distributions from parametric band-model fits to spectral data. This approach, which takes advantage of an analytic transmission function from which $f(k)$ may be derived, was employed by Lacis and Oinas [20], where Malkmus model parameters were least-squares fit to synthetic k-spectra. While the limitations of band-models may be overcome to some degree with this approach, discrepancies between Malkmus model and k-spectra derived k-distributions can exist, particularly where the distribution of line strengths within a band does not follow the form of the probability distribution function employed. While an approach such as this is an attractive hybridzation that combines the strengths of band-models and k-distributions, it remains essentially limited in its general applicability, in that it is impossible to know *a priori* whether or not the approximate nature of the fitting results will affect significantly the validity of the results obtained with their use.

Rigorously valid in the ideal case of homogeneous atmosphere, the k-distribution method has been extended to include the effects of pressure, temperature and optical path inhomogeneities on absorption processes as the so-called "Correlated k-distribution" (CKD) method. The fundamental assumption of this approach is that the ordering of the $k(g)$ appearing in each layer are "equivalent" in that radiative transfer calculations over some interval, Δg, are analogous to calculations over a physically equivalent (though not necessarily unique) set of wavenumber intervals throughout the depth of the atmosphere. The conditions under which this can be expected to occur are idealized. When applied to typical atmospheric spectra, a 'blurring' or anti-correlation of the relationship between k-distributions at different levels is usually observed. This phenomena occurs

as k-spectra at different heights are dissimilarly affected by temperature induced changes to line strength and by temperature and pressure induced changes to line broadening. As in Figure 3.2 where pressure and temperature-dependent blurring of k-distribution correlations are shown for the MAS Channel 40 H_2O band, it can be seen that both temperature and pressure inohomogeneities contribute to anti-correlations and that this blurring increases with difference in pressure and temperature. Asserting that these effects are commonly observed in the MAS band spectra, it is worthwhile to attempt an examination of the conditions under which they may affect the accuracy of raditive transfer calculations employing CKD.

Goody and Yung [12] demonstrate that CKD is exact under conditions where scaling approximations are obeyed. This 'similarity condition' is valid for bands composed of Doppler lines and strong Lorentz lines. They also show CKD to be exact for idealized Elsasser bands (where absorption lines are regularly or periodically spaced), Schnaidt models (where line overlap is treated as equivalent to line termination at some spectral distance $\pm\delta/2$), and for single-line models.

These idealized cases are not very satisfying when considering 'real' band absorption. More generalized proofs of the validity of CKD, as opposed to its exactness, are relatively straightforward to show in the assymptotic weak- and strong-line limits of absorption. Goody, *et al* [11] point out that in the strong-line limit absorption is dominated by centers of absorption lines, which do not change under conditions of LTE in the terrestrial atmosphere, and thus any anti-correlations that do occur are of negligible consequence. In the weak-line limit, transmission is by definition linearly decreasing with absorber optical path. Employing the approximation, $T = e^{-\epsilon} \simeq 1-\epsilon$, valid for $\epsilon \ll 1$, and the definition of the line brodening profile given in (2.22) the expression for the band-averaged line-by-line transmission through an inhomogeneous path,

$$\begin{aligned} T_{\overline{\nu}} &= \int_{\Delta\nu} \exp\left[-\int_{z_1}^{z_2} k(\nu', p, T)\rho \, dz\right] \frac{d\nu'}{\Delta\nu} \\ &= \int_{\Delta\nu} \exp\left[-\int_{z_1}^{z_2} \sum_i S_i(T) f_i(\nu', p, T)\rho \, dz\right] \frac{d\nu'}{\Delta\nu} \end{aligned} \tag{3.11}$$

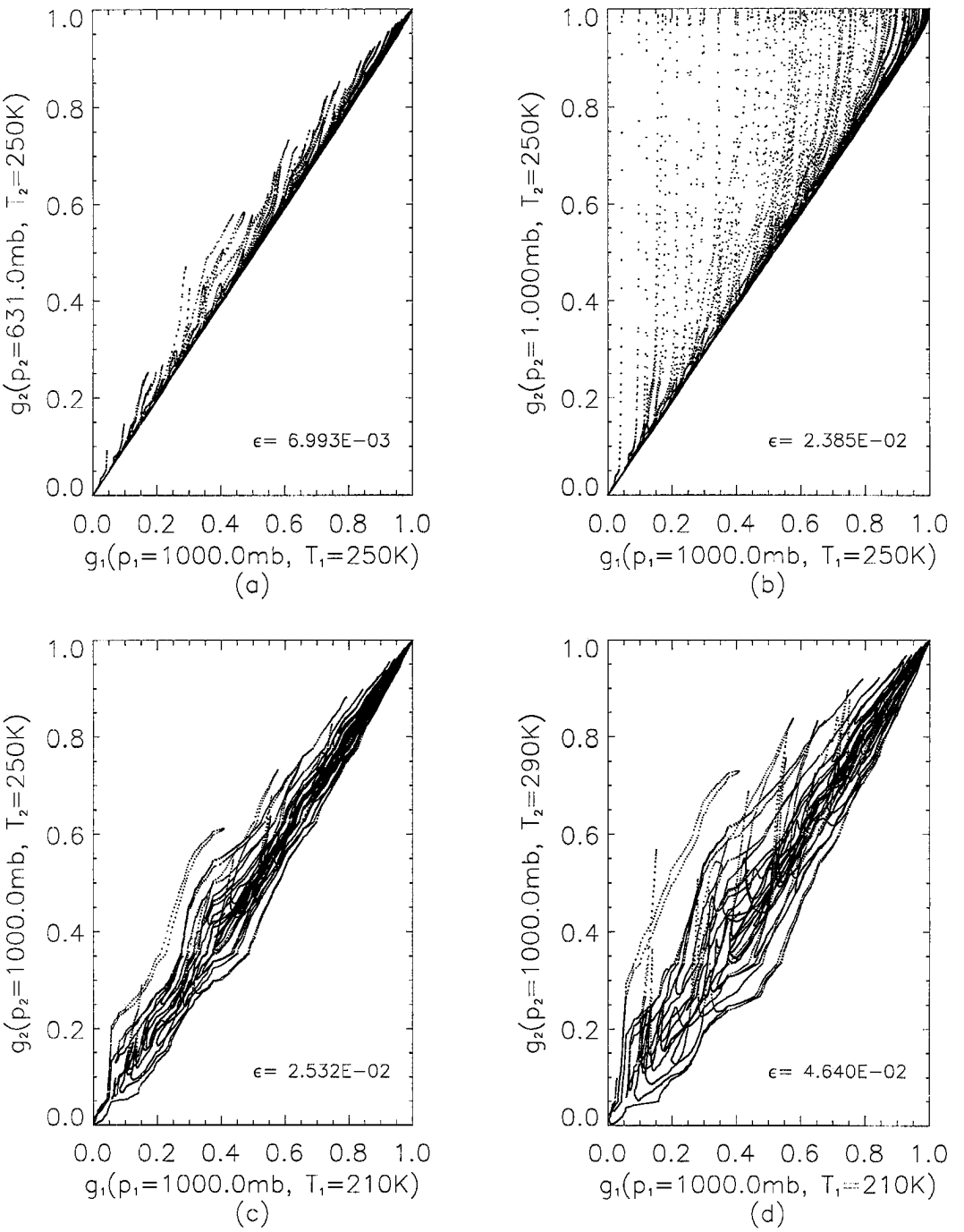

Figure 3.2: Blurring of correlations between MAS Channel 40 H_2O k-distributions due to pressure and temperature effects.. The point (g_1,g_2) is defined as $(g[k(\nu,p_1,T_1)]$, $g[k(\nu,p_2,T_2)])$ for each of the 45501 wavenumber intervals in the band. In (a) p_1 = 1000 mb, p_2=631 mb, $T_1 = T_2$= 250 K. In (b) p_1 = 1000 mb, p_2=1 mb, $T_1 = T_2$= 250 K. In (c) $p_1 = p_2$= 100 mb, T_1 = 210K, T_2=250 K. In (c) $p_1 = p_2$=1000 mb, T_1 = 210K, T_2=290 K. The appearance of 'paths' of dots arise from changes in the $g_{1,2}$ in the spectral vicinity of prominent absorption features. The ϵ indicate the average absolute differences between the $g_{1,2}$.

conveniently reduces to

$$\begin{aligned} T_{\overline{\nu}} &\simeq \int_{\Delta\nu} \left[1 - \int_{z_1}^{z_2} \sum_i S_i(T) f_i(\nu', p, T) \rho \, dz \right] \frac{d\nu'}{\Delta\nu} \\ &\simeq 1 - \int_{z_1}^{z_2} \sum_i S_i(T) \rho dz / \Delta\nu \\ &\simeq \exp\left[- \int_{z_1}^{z_2} k_{\overline{\nu}}(T) \rho dz \right] \end{aligned} \tag{3.12}$$

indicating that the $k(\nu, p, T)$ may be replaced by a single gray absorption coefficient, $k_{\overline{\nu}}(T) = \sum_i S_i(T)/\Delta_\nu$, which is a function of temperature alone. This then implies that anti-correlations are of no consequence, since for all ν and thus all g at any particular level, $k(\nu) \simeq k_{\overline{\nu}}$ and the CKD method is valid in the weak-line limit. A formal proof of the validity of CKD under the general case of absorption that is neither strong nor weak is not possible, since the numerically invoked Laplace transform is, by definition, not analytic. The validity of CKD under these circumstances (which are remarkably common in the 50 MAS bands) can only be assesed via comparisons with line-by-line calculations. A common practice in validating CKD models involves the comparison of line-by-line and CKD derived layer heating rates (e.g. Lacis and Oinas [20], Goody, *et al* [11], Fu and Liou [8], Kratz [16], [17]). Of the relevant literature reviewed in the course of the development of the approach taken here, several examples of CKD acheiving heating-rate results within 1 percent of line-by-line results were found. A genuine paucity of cases where CKD models produced large errors were found, and in the one case where such errors were addressed (Fu and Liou [8]), the effects of anti-correlations appear negligible relative to the choice of Δg quadrature intervals. A hypothesis which can only be tested empirically thus emerges: that anti-correlations, while a potential source of errors in CKD implementations, are less important than other factors that may cause the results obtained with their use to stray from validity. The determination of the role of anti-correlations in producing errors is fraught with difficulties, in that the parameters used are dependent on the atmospheric profile being modeled. A rather oblique examination of the role of anti-correlations, via the identification and elimination of errors from other sources, is attempted in the results section of the next chapter. Though annecdotal, this analysis indicates that in cases where

significant anti-correlations exist the validity of results are only marginally affected, and suggests that the mixing of spectral contributions in particular interval calcuculations through the depth of the atmosphere does not, in itself, adversely impact the validity of results at the band-wide scope.

3.4 Extensions to Overlapping Absorption: The Transmission Equivalence Concept and its Ramifications

Thus far, absorption by a single species in homogeneous and nonhomogeneous atmospheres has been considered. Typically though, more than one type of molecule actively contributes to absorption processes so that a means to describe this so-called *overlapping absorption* is required. Considering a mixture of two different gases, the spectral mean transmittance, following from Lambert's law, is

$$T_{\overline{\nu}}(1,2) = \int_{\Delta\nu} T_\nu(1) \times T_\nu(2) \frac{d\nu}{\Delta\nu} \tag{3.13}$$

Transmission equivalence, which is valid in bands with constant sources if $T_\nu(1)$ and $T_\nu(2)$ are uncorrelated in frequency space, is formally expressed as

$$\begin{aligned} T_{\overline{\nu}}(1,2) &= \int_{\Delta\nu} T_\nu(1) \frac{d\nu}{\Delta\nu} \times \int_{\Delta\nu} T_\nu(2) \frac{d\nu}{\Delta\nu} \\ &= T_{\overline{\nu}}(1) \times T_{\overline{\nu}}(2) \end{aligned} \tag{3.14}$$

The validity of transmission equivalence has been shown in specific line-by-line calculations over a relatively narrow 5 cm^{-1} spectral interval centered near 15 μm (Ackerman [1]), where transmission differences of less than 1% were found for calculations using the forms of (3.13) and (3.14) for overlapping CO_2 and H_2O absorption. Fu and Liou [8] examined the use of transmission equivalence for three different bands, comparing CKD and LBL results for cases of overlapping absorption by 1, 3, and 5 different species and also found good agreement for the two approaches. Given these results, albeit annectdotal in nature, the approach to transmission equivalence defined in (3.14) does not appear to present problems, *per se*. In the visible through far-IR spectrum, however, source terms often vary to the degree that parameterizing them as constant over a band has the potential to introduce significant errors, examples where this isn't the case not withstanding.

A common practice toward implementing (3.14) (e.g. Fu and Liou [8], Kratz [16]) has been to produce a set of k-distributions at sets of reference levels and temperatures, to then determine Δg interval-specific layer optical depths via interpolation and/or polynomial fitting to layer-specific temperatures and pressures, while conducting $\Pi_i M_i$ radiative transfer calculations, where M_i is the number of interval quadrature points required for *each* absorber. For example, in the case of some arbitrary radiative transfer calculation, $\mathcal{RT}$, involving 3 overlapping absorbers, with M_1, M_2, and M_3 intervals respectively, the final result, $\mathcal{RT}_{final}$, is the compound interval width weighted sum of $M_1 \times M_2 \times M_3$ individual radiative transfer calculations, i.e.,

$$\mathcal{RT}_{final} = \sum_{i}^{M_1} \sum_{j}^{M_2} \sum_{k}^{M_3} \mathcal{RT}(i,j,k)\ \Delta g_1(i)\ \Delta g_2(j)\ \Delta g_3(k) \tag{3.15}$$

where, the gaseous optical depth in some arbitrary layer, ℓ, in the $(i,j,k)^{th}$ calculation interval is determined as

$$\tau^{\ell}(i,j,k) = \tau_1^{\ell}(i) + \tau_2^{\ell}(j) + \tau_3^{\ell}(k) \tag{3.16}$$

The interval results weighting scheme described by (3.15) ensures that $\sum(\Pi\Delta g) = 1.0$, such that the contributions of the absorber-specific τ^{ℓ} contributions to radiative transfer within the band are appropriately weighted. However, the inherent mixing and re-use of interval- and absorber-specific optical depths in separate calculations is a disturbing feature of this approach. In the example above, the optical depth of the 1^{st} absorber in the i^{th} Δg_1 interval is used $M_2 \times M_3$ times, i.e., across the whole of $\Delta g_1(i)$-weighted g-space for absorbers 2 and 3. Thus, in overlapping absorption bands where features of the individual absorbers occur in different spectral sub-regions within the band, Δg space mixing of physically unrealized combinations of absorption coefficients will inevitably result. Transmission equivalence as employed in (3.15), implies that such mixing will not, by itself, give rise to large errors in absorbing atmospheres, but its use also requires the use of band-averaged source functions which results in the loss of other interval-specific features that may be important sources of errors. These problems can be overcome to some degree by splitting bands into sub-bands small enough to validate source function

averaging and to resolve important non-overlapping absorption features, but only at the computational cost of the additional interval calculations that are usually required.

A more spectrally precise description of the effects of other optical properties contributing to radiative transfer, for example those arising from the inclusion of clouds and aerosols, whose changes in wave-space are perhaps of secondary import in most spectral regions, may also improve forward modeling fidelity when determined at the interval-specific as opposed to the band-averaged level. While these sources of potential pitfalls to forward modeling can also be overcome, where necessary, by appropriate combinations of sub-band calculations as above, yet another complicating factor to the creation of accurate CKD and ancillary parameters is introduced by their consideration.

A recently developed approach to band-modeling which, like the k-distribution, makes use of a Laplace transform of a function of frequency is discussed by Tjemkes and Shmetz [31]. In their approach, a sample of equally spaced line-by-line radiances resulting from overlapping absorption processes are transformed to estimate a cumulative radiance-probability distribution. Refered to as the Radiance Sampling Method (RSM), results obtained with this approach are shown to converge to the results obtained with the full set of wave-space intervals with increasing ΔI quadrature points. This strictly monochromatic method produces none of the errors associated with the transmission equivalence approach to overlapping absorption, and allows the direct incorporation of other spectrally dependent quantities, such as the ISR. While it is typically more than an order of magnitude more computationally efficient than optimized line-by-line methods, RSM still requires a few hundred to several hundred individual radiative transfer computations to represent accurately instrument measured radiance fields.

3.5 Implementation Overview

Upon consideration of the factors which complicate the validity of CKD parameterizations, and while still requiring maximum computational efficiency, an approach that incorporates spectral information and isolates overlapping absorption at the Δg interval-specific level would then seem superior to the conventional CKD approaches described above. First,

it would serve to simplify the creation process. By incorporating spectral information at the interval level, time-consuming examinations of the sources of errors arising from band-averaged parameters and the duplication of effort involved in the creation of sub-bands to overcome them can usually be avoided. It is conceivable that cases may arise where the improvements that result from transfering the spectral averaging and features of overlapping absorption from the band to the interval level may be insufficient to obtain the fidelity required. In these circumstances, it is still possible to resort to band-splitting (and appears to be the only remedy), but the relative frequency of this necessity should be lower than with conventional CKD approaches. An appropriately designed data structure that incorporates all of the spectral information and meta-information relevant to the radiative transfer process in bands with arbitrary absorption, scattering, source function and instrument sensitivity features is then a potentially valuable contribution to the field of forward radiative transfer modeling. The positive effects on the fidelity of remote-sensing observing systems, and the gains in the computational efficiency and physical validity of band radiation schemes employed as components of other atmospheric models justify the additional book keeping involved in the creation process.

The novel approach to CKD parameters creation developed in this study, followed just such an interval-level philosophy. A recursive approach to overlapping absorption in a spectral-space tracking k-distribution creation process was employed. This concept grew from a k-distribution approach for homogeneous singly-absorbing atmospheres first articulated by K.F. Evans (personal communication). Here, this concept is extended to accomodate overlapping absorption in inhomogeneous atmospheres. In the case of a band with more than one active absorber, the absorbers are first sorted into increasing column transmission order, and the strongest absorber is considered first. Reference k-distributions are then created from the k-spectra for the first absorber at the 26 standard pressure levels at 250K, according to the forms described by (3.3) and (3.4). An error minimization scheme, discussed in detail in the next chapter, is then employed to determine the set of Δg intervals required to produce a set of parameters meeting complimentary transmission and relative absorption error criteria over a range of optical paths likely to be

encountered in the terrestrial atmosphere. Upon succesful minimization, the wavenumber intervals composing the 1^{st} Δg-space interval are then used to create k-distributions, normalized by the bandwidths they represent, for the 2^{nd} strongest absorber. This process continues through the each of the intervals created by the process itself, until all of the intervals relevant to each absorber have been successfully determined. At this point, a heirarchy of Δg intervals that descend a tree of absorbers exists. Considering each absorber as a level of recursion, the wavenumbers composing each of the intervals for the last absorber, or lowest level, are recovered along with the products of the Δg intervals used in descending the levels. These data are then used to create a set of lowest-level Δg intervals, and interval effective absorption coefficients corresponding to each absorber as functions of the set of reference temperatures and pressures. Since the wavenumbers composing each interval are known, interval averaged ISRs, mean wavelengths, and interval-specific ISR weighted-average source terms are then determined, such that a full suite of interval-specifc information is available. These data are then saved in a platform and programming-language independent data structure format[1] that is easily implemented into arbitrary radiative transfer schemes.

3.6 Summary

In this chapter, a review of approaches to describing the effects of gaseous absorption processes in radiative transfer modeling was undertaken. Throughout this discussion the fundamental conflict between accuracy and computational efficiency is a common theme. This conflict serves to either complicate or eliminate the general applicability of each of the conventional methods described. While conventional CKD approaches overcome the problems inherent to band-averaged modeling approaches to some degree, and are more generally applicable than band-models, they come with the loss of potentially important spectral information that can only be partially regained by compromising computational

[1]The corresponding ".ck" data structure format and supporting interface routines are described in detail in Appendix A.

efficiency. Line-by-line modeling, and clever optimizations of this most computationally expensive approach, while the most accurate way to describe radiative transfer, simply require too much effort to be practicable in schemes requiring a large number of band radiances. The novel approach developed in this study appears, from a theoretical standpoint, to offer a comprimise which satisfactorily resolves the conflicting interests of modelers. It appears generally applicable to any radiative transfer modeling scheme, and as such, represents a potentially significant contribution to the field.

Chapter 4

The k-Parameters Creation Process

Having introduced the recursive approach to the creation of Correlated-k parameters that retain interval-averaged spectral information, the detailed description of their creation is the subject of this chapter. The focus here shifts from the development of radiative transfer theory concerning gaseous absorption processes to the details of the application responsible for producing the k-parameters data structure that can then be employed in radiative transfer calculations. As such, much of the vocabulary used in the following discussion is more closely associated with computer science and programming logic than radiative transfer, though the physical considerations which serve as the basis of the application remain relevant throughout.

The application that produces k-parameters is written in IDL. This programming environment, which is primarily a tool for the visualization of data, is relatively easy to work with, and permits the simple integration of calculations and results plotting codes. While IDL is a run-time interpreted language, which implies that code written with it will run somewhat slower than equivalent compiled language algorithms, it offers a large selection of numerical procedures that would be tedious to port, as well as many 'built-in' calculation and data manipulation functions. These built-in functions are highly optimized assembly language routines offering performance that would be difficult match in anything but similarly coded implementations. The combination of ease of use and good performance in computationally intensive tasks associated with the k-parameters creation process justify the use of IDL.

An algorithm that creates absorber sub-intervals, via an iterative approach that tries to minimize transmission and relative absorption errors, is at the center of the application.

Here 'interval' refers to the subset of k-spectra appropos to the Δg interval result from the last higher-level minimization that is under consideration, or in the case of a top-level minimization, the entire band, and 'sub-intervals' refers to the set of Δg intervals that result from applying the minimization scheme to them. Starting with one or more sets of 78 k-spectra, this collection of programs works its way through the absorbers, and produces a parameters data file, refered to as the '*.ck*' file because of its file name suffix, containing all of the information required to perform radiative transfer calculations.

The application is designed, through the use of appropriate data structures, to be flexible and generally applicable enough to handle bands with an arbitrary number of absorbers. The only real consideration in its use is the amount of available disk space to hold interim results. Even after nearly a year of development, it remains an incomplete application, in that certain combinations of strong absorbers may require several runs of the application to get it to complete, and the resultant parameters require empircal validations that are only annectodal indications of their validity. However, its general robustness, as indicated by the results to be shown in the next chapter, speaks to both the soundness of the theory behind it and the consideration given to details during the application development process.

In this chapter, the entire application is explained. A program that manages the creation and validation of the *.ck* parameters file, as well as the associated data structures that lend it much of its flexibility, are first described in order to put the sub-programs that this top-level program calls to do specific tasks in their appropriate contexts. The details of the error minimization scheme are then discussed, followed by a description of the programs which use the results of the minimizations to create the *ck* files.

4.1 Top-level Controlling Program and Associated DBMS Structures

A controlling process for the band as a whole was developed in order to automate, and thus expedite the parameters creation process. This algorithm does much of the work not directly related to the creation of sub-intervals. Specifically, it performs, or calls other programs to perform the following tasks:

- Initialize data elements related to the band as a whole and to each absorber.
- Manage the minimzation processes via a recursively called sub-procedure which, at each invocation:
  - Creates k-distributions from appropriate k-spectra subsets.
  - Calls the minimization processes with the appropriate parameters.
- Manage the creation of the output *.ck* parameters data file.
- Perform and plot the results of validation tests of the resultant *.ck* parameters file.

This process is facilitated through the use of a relational Data Base Management System (DBMS) that integrates elements from the band-wide through sub-interval specific scopes. The data files follow a nomenclature that uniquely identifies the instrument-channel combination they are associated with and, where appropriate, a specific absorber. The data types contained in the file are identified via a file name suffix. At the top of the heirarchy is the band definition, or *.ckinf*, file which contains the band begining and ending wavenumbers, the resolutions used to create k-spectra, and the standard HITRAN identification numbers associated with each molecular specie that is active within the band. Related band-wide definitions data include the absorber line strength cutoff values, which are stored in absorber specific *.ckinf2* files, and a file containing estimated column transmissions associated with each absorber. These transmission data were determined from 1976 US Standard Atmosphere column paths and the 631.0 mb/250 K k-spectra. The first of these two files is used to optimize the k-spectra creation process, while the second is used to determine the ordering of absorbers in the k-parameters creation process. The creation of the second file serves to filter out from consideration those absorbers with negligible contributions to absorption processes.

Upon starting the k-parameters creation process, the controlling program reads and stores the *.ckinf3* data, and checks for the existence of the k-spectra files that the data indicate are required. If they are all present, the program proceeds to call a sub-process that allows the user to change a set of default parameters associated with each absorber.

These *minimization criteria* are then used in the minimization scheme. Stored in a band *.mincrit* file, these data include specifications of the maximum number of Δg sub-intervals, and the maximum allowable sub-interval averaged transmission and relative absorption errors used to determine the minimization status of sub-intervals. The maximum allowable values of these two quantities as applied to individual transmission calculations are also stored here, along with a value specifying an acceptable range in the relative absorption maxima across the resultant sub-intervals.

When these initialization tasks are completed, a recursively invoked procedure is then called to manage the sub-intervals creation process. Its algorithm varies somewhat between top-level and subsequent level invocations. At the top-level, the complete set of wavenumbers in the k-spectra associated with the absorber are employed, while lower-level calls will employ subsets of the band associated with the specifc Δg interval of interest. In lower-level calls, the procdure also first checks for and loads minimization results from the last level. In either the top-level or lower-level invocation cases, it then checks for minimization results at the called level, and if they already exist, the minimization process is skipped, and the code loops over the number of Δg subintervals and calls itself with parameters specifying the results of each Δg subinterval at this level in order to perform a minimization at the next level. By doing this, the k-parameters creation process can relatively quickly pick up at the place it left off in the case of encountering some critical error. A nomenclature that uniquely specifies the level and Δg interval appropos to minimizations is employed to name minimization results and related data files. An example of this nomenclature is represented in Table 4.1, where the heirarchy associated with MAS channel 40 is shown. The top-level, associated with H_2O, carries the instrument-channel combination band name, while subsequent levels also indicate the combination of higher level intervals from which they were created. For example, the specifier 'mas40.5.1' indicates that the subset of k-spectra from which k-distributions and subsequent interval minimization results were derived, employ wavenumbers appearing in the second sub-interval (intervals are numbered starting at 0) of the minimization performed using the wavenumbers appearing in the sixth Δg interval of the top-level minimization.

Absorber →	H_2O	CO_2	O_3
Level →	1	2	3
	mas40		
		mas40.0	
			mas40.0.0
		mas40.1	
			mas40.1.0
		mas40.2	
			mas40.2.0
		mas40.3	
			mas40.3.0
		mas40.4	
			mas40.4.0
		mas40.5	
			mas40.5.0
			mas40.5.1
		mas40.6	
			mas40.6.0
		mas40.7	
			mas40.7.0

Table 4.1: Recursive minimization heirarchy for MAS channel 40 k-parameters creation. The error minimization scheme begins with entire band and the results are stored in files prefixed with 'mas40'. The wavenumber intervals composing the first Δg interval in 'mas40' are then used in the first minimization of CO_2 k-spectra and the results are stored in 'mas40.0' files, and so on.

Upon reaching a called Δg interval where no minimization result exists, k-distributions for each of the standard pressure levels are created using the subset of 250K k-spectra wavenumbers appearing in the Δg interval from the previous level's minimization. The binning and summing approach to the creation of k-distributions, defined in (3.3) and (3.4) is conceptually equivalent to a histogram, and permits the use of IDL's built-in HISTOGRAM() function. This function allows arguments specifying a vector of $\Delta \log_{10} k$ bin definitions from which the density function is computed, and permits the return of so-called *reverse indicies* that may be used to determine the wavenumber intervals composing each $f(k)$ bin. It was found that the routine written to create k-distributions from a passed set of wavenumber intervals employing HISTOGRAM() performed at a approximately 25 times faster than similar code writen in the C programming language. The resultant k-distributions and bin-ordered wavenumber indicies are saved in separate files, and the minimization process, as described in the next section, is then invoked. Upon successful completion, a loop over the resultant Δg subintervals is invoked, and the wavenumber intervals corresponding to each Δg subinterval are then used to call next level of recursion. When this loop completes, or in the case of having reached the lowest level of recursion, the function returns to the previous level and the process continues until all of the wavenumbers for all of the absorbers have been successfully transformed to Δg subintervals.

When all Δg intervals have been successfully minimized, the controlling process proceeds to call another routine to create the *.ck* parameters file, a validation test is performed and the results are plotted. This recursive approach, and the data structures associated with it, while perhaps being somewhat difficult to understand at first, offer the flexibility required to handle bands with an arbitrary number of absorbers, and when implemented in a way that only the minimal set of information required is retained in memory at each level of recursion, ensures that it is applicable to bands that requiring many levels and/or minimizations.

4.2 Subintervals Error Minimization Process

The sub-intervals determination program attempts to minimize transmission and relative absorption errors for a given set of k-distributions. These complementary criteria evolved over the course of the application's development, during which is was found that they were individually insufficient to insure accurate results throughout the depth of the atmosphere. The iterative approach of the program starts with a single Δg interval using the complete set of bins in the k-distribution, and adds or adjusts the boundaries of sub-intervals as required to acheive the minimization criteria specified.

4.2.1 Transmission Calculations Definitions

At the heart of this process is the evaluation of a pair of transmission calculations at each standard pressure level over a sample of paths that may be encountered there. The first of these calculations determines the j^{th} interval-averaged transmission for each path by integrating over each of bins falling within the j^{th} subinterval as

$$T_{k(g)}(j, p_{std}, u) = \left\{ \sum_{i=bin_0}^{bin_1} \exp\left[-k(p_{std}, g_i)u\right] \Delta g_i \right\} / \sum_{i=bin_0}^{bin_1} \Delta g_i \tag{4.1}$$

where bin_0 and bin_1 correspond to the k-distribution elements with $g_0(j) \leq g < g_1(j)$, and Δg_i is the specific bin width in g-space. The second calculation employs a subinterval-width weighted average value of the absorption coefficient, determined as

$$k_{eff}(j, p_{std}) = \left\{ \sum_{i=bin_0}^{bin_1} k(p_{std}, g_i) \Delta g_i \right\} / \sum_{i=bin_0}^{bin_1} \Delta g_i \tag{4.2}$$

in a single transmission calculation, where

$$T_{k_{eff}}(j, p_{std}, u) = \exp\left[-k_{eff}(j, p_{std})u\right] \tag{4.3}$$

The path-averaged differences between (4.1) and (4.3) then serve to define the errors associated with each interval. The use of these error values and the adaptive behavior they force are discussed in further detail below.

4.2.2 Optical Path Sample Determination

Given the nonlinear form of the changes in the transmission values determined from (4.1) and (4.3) with changes in optical path, the choice of the specific sample of paths to be used is of primary importance to the validity of the resultant k-parameters. To be universally applicable, path samples might include values producing transmissions from the linear through the strong-absorption regimes. However, this approach can produce interval statistics indicating large errors, significant contributions to which arise from the use of sample paths at levels in the atmosphere where they could not physically occur. In this study, the paths used in determining the errors associated with Δg intervals were adapted to be representative of the range of values likely to be encountered in their use in radiative transfer calculations. For each of the 26 standard pressure levels, a distinct sample of paths were determined for each absorber. This approach seeks to provide a *representative* sample as opposed to a *universal* sample, and is justified for the following reasons:

- Multiple scattering effects and variations in solar zenith angle which tend to increase photon path lengths through an layer, and thus the effective layer optical depth, have been used to justify the use of *universal* path samples (e.g. Kratz, [16]). In modeling, these effects are usually described in terms of a vertical path optical depth. To the degree that these vertical path optical depths are accurate, the effects of multiple scattering and slant-path optical depths will also be accurately determined.

- Unrealistic optical paths serve only to skew the statistics applicable to realistic optical paths, and as such, will actually *decrease* either the validity or computational efficiency of the results obtained with their implementation. In the upper atmosphere in particular, the use of universal paths will tend to overemphasize the errors associated with physically unrealizable cases of strong absorption, and thus require the creation of more intervals (and thus more computational effort when employed in models) to ensure the validity of calculations involving profiles that will never be used.

The paths applicable to the specific absorber-reference level combinations were determined from a set of standard atmospheric profiles that includes the 1976 US Standard Atmosphere (NOAA, [24]), containing profile information for 11 different absorbers, and the collection of so-called *McClatchey profiles* (McClatchey, *et al* [22]), containing profile information for water vapor and ozone in 7 atmospheres applicable to different latitudinal zones and times of the year. For each of the 26 standard levels, a sample of 20 reference paths were created, as follows, and stored in an ancillary data file. A minimum path, u_{min}, was determined by taking the lowest path density, in g/(cm^2 km), occuring in the set of available profiles, nearest to the standard level and multiplying it by a relatively thin 100 meter (0.1 km) thickness. A maximum path, u_{max}, was then determined by integrating the maximum path densities occuring in the set of profiles over the range of levels applicable to a layer with an average pressure close to the standard pressure level. For example, the maximum path for the 0.251 mb H_2O standard level was determined by by integrating the McClatchey Tropical profile path density from the top of the atmosphere (TOA), at 100km, to the nearest level below 2x0.251 mb, here 0.854 mb, and then multiplying this path by a factor of 2.5 to accomodate exceptional cases. The range in paths at each standard pressure level in terms of their natural logarithms, ln $u_{max}(level)$ - ln $u_{min}(level)$, was then used to determine the sample of paths at each standard level as

$$u(level, i) = u_{min} + i \times \exp\{[\ln u_{max}(level) - \ln u_{min}(level)]/19\} \tag{4.4}$$

where i represents the path sample number and varies from 0 to 19. Since transmission is a exponentially decreasing function of absorber path, this sample selection process provides a physically representative set of equally spaced points in transmission space, over which the accuracy of the $[k_{eff}(j, p_{std}), \Delta g_j]$ combination may then be evaluated. This approach is still rather generous, in terms of the profiles with which the parameters may eventually be used, but unrealistic paths are mostly eliminated from consderation. The sample of paths used in minimizations of H_2O k-distribution errors is shown as a function of the standard pressure levels in Figure 4.1. The samples employed for other molecular species follow a similar trend in range with pressure.

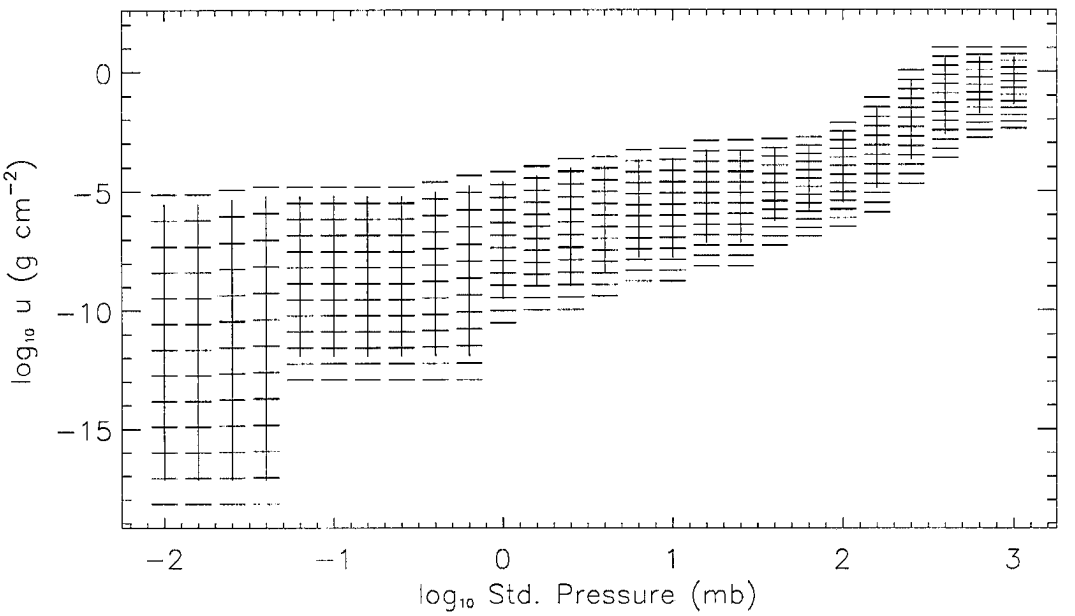

Figure 4.1: Minimization H_2O path samples as $f(p_{std})$. Horizontal lines indicate discrete path values employed at each standard pressure level. Vertical lines indicate the range in applicable paths determined from the set of McClatchey and 1976 U.S. Standard Atmosphere profiles.

4.2.3 The Use of Minimization Criteria

The transmission values determined from (4.1) and (4.3) are used to determine path-averaged transmission and relative absorption error statistics for the j^{th} interval as

$$\bar{\epsilon}_a(j) = \frac{1}{N_1} \sum_{p_{std}} \sum_{u} \left| T_{k(g)}(j, p_{std}, u) - T_{k_{eff}}(j, p_{std}, u) \right| \tag{4.5}$$

$$\begin{aligned} \bar{\epsilon}_r(j) &= \frac{1}{N_2} \frac{\sum_{p_{std}} \sum_u \left| (1 - T_{k(g)}(j, p_{std}, u)) - (1 - T_{k_{eff}}(j, p_{std}, u) \right|}{\sum_{p_{std}} \sum_u (1 - T_{k(g)}(j, p_{std}, u))} \\ &= \frac{1}{N_2} \frac{\sum_{p_{std}} \sum_u \left| T_{k_{eff}}(j, p_{std}, u) - T_{k(g)}(j, p_{std}, u) \right|}{\sum_{p_{std}} \sum_u 1 - T_{k(g)}(j, p_{std}, u)} \end{aligned} \tag{4.6}$$

where the sum in (4.5) is over the complete set of $N_1 = 26 \times 20 = 520$ transmission calculations, and the sum in (4.6) is over the set of N_2 transmission calculations where $0.00001 \leq T_{k(g)}(j, p_{std}, u) \leq 0.9999999$. The distinction between the samples used to create these statistics arises from the need to eliminate from consideration very small absolute transmission errors that produce large relative absorption errors, which inevitably occur

Interval Error Statistic	Interval Status
$\bar{\epsilon}_a \geq \bar{\epsilon}_a^c$	*'bad1'*
$\bar{\epsilon}_a \geq 2 \times \bar{\epsilon}_a^c$	*'bad2'*
$\bar{\epsilon}_r \geq \bar{\epsilon}_r^c$	*'bad3'*
$\bar{\epsilon}_a < \bar{\epsilon}_a^c$ and $\bar{\epsilon}_r < \bar{\epsilon}_r^c$	*'good1'*

Table 4.2: Minimzation interval status definitions. The individual status definitions are determined from user-supplied maximum allowed interval average transmission error, $\bar{\epsilon}_a^c$ and maximum allowed interval average relative absorption error, $\bar{\epsilon}_r^c$, criteria.

in the limit $T_{k(g)}(j, p_{std}, u) \rightarrow 1.0$, coupled with the desire to remove relatively insensitive saturated paths from consideration. The inclusion of these neglected sample would result in overestimates and underestimates of $\bar{\epsilon}_r$ in the limits of weak and strong absorption, respectively.

After determining the error statistics for each interval, the values are used to determine the *status* of each interval. These interval statae are then used to determine the action, if any, to take in order to set up the next iteration. Intervals are tagged with one of four statae, as indicated in Table 4.2. The error statistics and interval statae are jointly used in a two-level minimization scheme. The first level of minimization seeks to create a set of Δg intervals satisfying the average transmission error criterion chosen by the user. That is, a set where each interval, and the sub-band as a whole have status *'good1'* or *'bad3'*. When this is achieved, a second level of minimization commences. This minimization attempts to reduce the range in the maximum values of the ϵ_r encountered in each interval across all intervals, standard levels, and paths, to the user-specified $\Delta\epsilon_r^c$ criteria. The first level of minimization, then, serves to produce a set of intervals that will, on average, produce satisfactory results, while the second level of minimization serves to decrease the probability that outlier profile paths will have an adverse effect on the validity of optical depth calculations. This serves to ensure that all of the Δg intervals will be roughly equally valid (or invalid) over the range of paths likely to be encountered.

A hard-coded set of *action rules*, employing the minimization criteria in conjunction with the set of interval and sub-band error statistics determines the action or actions to take subsequent to their determination. Developed over the course of the development of

the application, they reflect both the core set of minimization goals, and optimizations to the process that help speed convergence to these goals. When an interval fails to meet the criteria appropos to the level of minimization, the only way to improve it is to shrink its size in g-space, and thus decrease the range in k over which it applies, such that the single valued k_{eff} does not produce as significant error values over the range in u as it would otherwise. In the first level of minimization, when there are any intervals with status *'bad1'* or *'bad2'*, the one with the worst $\bar{\epsilon}_a$ is chosen as the *active* interval. The size of the interval in g-space is then reduced by some *adjustment factor*, $0 \leq f < 1$, so that in the next iteration, the interval has $\Delta g_{i+1} = f \times \Delta g_i$. The value of f used is an optimization depending on the minimization level and the interval status. Since an interval with *'bad2'* status generally needs to be shrunk more than an interval with *'bad1'* status, a factor of 2.5 is applied to the adjustment factor for such intervals. During the second level minimization, which is essentially a 'fine-tuning' of level 1 results, a host of factors come into play, including how the last iteration changed the set of interval and sub-band averaged results relative to the iteration before. The convergence to or divergence from the desired result is used to determine the adjustments to interval boundaries that result. When an iteration at this level produces negligible change in results, the adjustment factor is doubled, up to a maximum of 16% of the interval width, so that the code does not spend an inordinate amount of time trying to improve a single interval. Similarly, when an iteration actually increases the spread in errors, via 'overshooting' the optimal boundaries, the boundaries are reset to those of the previous iteration, f is halved and the interval-adjustment is repeated.

Returning to the Level 1 minimization for a moment, when none of the intervals have *'good1'* status, the only way to improve results is add another interval. The interval with the worst statistics is then chosen for splitting. Problems were encountered when the recursive approach was developed, especially in the lower-level minimizations of higher-numbered Δg intervals from previous absorbers. In these situations, the k-distributions become relatively coarsely resolved as the size of the sample of wavenumbers composing them shrink. A partial solution to this problem involved increasing the k-distribution bin

resolutions, up to 1000 bins per decade k, but in some circumstances the phenomena of splitting an interval in a way that no bins ended up in one of the resultant two intervals still occured. The way in which the $\log_{10}\Delta k$ bins are defined serves to resolve stronger absorption coefficients more finely, so a means to overcome this problem was found by splitting bins unequally. Currently, bins are split via 3:1 Δg fraction process such that 75% of the bins end up in the lower-numbered resultant subinterval. This overcomes all but the most obstinate sources of this error which occur in cases where a Δg interval that is chosen for splitting is composed of just a few bins[1]. When such intervals are still bad, they are simply removed from consideration in further iterations, since generally, even though error prone, they will contribute only negligibly to the errors in the band as a whole. During the MAS parameters development, only one case of running out of intervals to adjust through this process was encountered, and it was finally minimized by increasing the bin size to 2000 per decade k.

The way in which g-space is redistributed after an interval size adjustment has been determined is also an optimization to the minimization scheme. When interval numbers 0 or 1 are adjusted, the remaining g-space is added to all of the other intervals in proportion to their size. The redistribution of g-space for higher numbered intervals is handled differently, in that the g-space is redistributed amongst intervals with numbers less than the active interval in proportion to their size. By doing this, convergence to minimization criteria is quickened in two ways. First, since higher-numbered interval boundaries remain the same, transmission calculation results from the previous iteration may be retained, saving the computational effort that would be wasted in duplicating results. Second, a successively finer scale adjustment scheme may be used such that the focus of improvements usually works its way from higher-numbered intervals to lower numbered intervals. Each time either interval 0 or 1 are set as the *active* interval, f is slightly reduced, so that on the next pass through the intervals, a convergence to the level 1 minimization goal is more likely.

---

[1]By definition intervals composed of just one bin will have exactly the same $T_{k(g)}$ and $T_{k_{eff}}$ results and thus be error free.

During the level 2 minimization, in addition to determining the 'worst' interval, the 'best' interval is also identified, so that intervals that are statistical outliers in either the good or bad sense are relatively quickly brought into the fold of the group of sub-band intervals. An outlying *'good1'* interval may also be selected as *active* and its Δg *increased.* This often results in a reduction of the overall sub-band averaged errors, and those of many of the rest of the intervals as well.

Occasionally, the minimization process will not be able to meet the complementary set of criteria specified for the absorber. Examples of such circumstances include requiring more intervals than the *.mincrit* parameters specify, running out of adjustable intervals, or not being able to meet one or both of the level 1 and level 2 goals in the number of iterations allowed. The minimization program always returns to the caller with a integer value containing bitwise codes indicating the set of conditions at the time of exit. These data may then be used by the user to adjust the appropriate criteria in order to acheive a satisfactory minimization. The structure and logic of the recursive process will cause the k-parameters creation application to restart at the specific minimization where it left off, upon adjusting the minimization criteria and re-running the application.

4.3 Parameters File Creation

When all of the minimizations required as result of the minimization process itself have successfully completed, the recursive procedure will return to the controlling process described in §4.1. At this point there may be as many as several dozen minimization results, each containing sub-intervals data pertaining to 26 minimized k-distributions. The next step in the k-parameters creation process is to pull these results together and put them into a format usable by radiative transfer models. These data are compiled into the *.ck* parameters file. The details of the format of this file type are listed in Appendix A, though it remains to define the meaning of its contents. Within the *.ck* file creation process are three separate sub-processes: the determination of the set of k_{eff} parameters applicable to layers with arbitrary p_{av}, and T_{av} state values; the determination of ancillary interval central wavelength, interval average ISR, and parameters for use in determining interval

specific source terms; as well as the *.ck* file writing process itself. These three sub-process can be seen to be peratain to absorber/interval-specific parameters, interval-specific parameters, and band-wide parameters, thus the organization into 3 separate sub-programs.

The first of these subprograms determines the absorber/interval-specific k-parameters. After having determined the complete set of applicable lowest-level minimization results, they are sorted into a logical name-order, and a loop over them is begun, within which exists another loop over the number of sub-intervals particular to the minimization of interest. At each iteration in this inner loop, a third loop over the standard pressure levels is used to first identify the wavenumbers composing the lowest-level subinterval of interest. This is accomplished by derefrencing the bin to wavenumber interval indicies created as part of the k-distribution creation process. Then, looping over the number of absorbers in the band, the interval-averaged k_{eff} for each absorber at each of the standard pressure level and temperature combinations within the subinterval are determined from the corresponding N_l k-spectra elements as

$$k_{eff}(i,j,l,T_{std}) = \frac{1}{N_l}\sum_{m=1}^{N_l} k(\nu_m,l,T_{std}) \tag{4.7}$$

where j represents the final calculation interval number, i represents the absorber number employed i^{th} recursion level, and l is the standard pressure level number. Typically, the N_l are the same to within a few wavenumber intervals across standard pressure levels, though the specific wavenumber intervals composing each set may be increasingly disimilar with physical separation.

The set of three k_{eff} for a given standard pressure level are then fit to a set of three quadratic polynomial coefficients of a function of $(T-250K)$, from which the k_{eff} at a standard pressure level may then be determined at arbitrary temperatures between 210K and 290K as

$$k_{eff}(j,i,l,T) = k_{eff}(j,i,l,250K) \times [a_0 + a_1(T-250) + a_2(T-250)^2] \tag{4.8}$$

Results are checked to ensure that the regression does not produce negatively valued k_{eff} over the range of T for which they are ostensibly valid. In the relatively rare cases where

this does occur, as a result of changes in the $k_\nu(T_{std})$ that are not adequately described by the quadratic fit, a simpler linear regression, of the same form, such that $a_2 = 0$, is used instead. This process results in a set of $k_{eff}(250K)$ and corresponding temperature adjustment coefficients for each of the set of standard pressure levels, which at the interval/absorber level is similar to those developed by Fu and Liou [8], and Kratz [16]. Following their common approach to applying these parameters in radiative transfer models, for a layer with $p_{std}(l) < p_{av} < p_{std}(l+1)$, the interval/absorber specific optical depth contribution is determined by linearly interpolating in pressure the pair of $k_{eff}(j,i,l,T_{av})$ determined from (4.8). That is, for the n^{th} layer in a model profile,

$$\begin{aligned} k(j,i,p_{av}(n),T_{av}(n)) &= k_{eff}(j,i,l,T_{av}(n)) + \left[\frac{p_{av}(n)-p_{std}(l)}{p_{std}(l+1)-p_{std}(l)}\right] \times \\ &\quad [k_{eff}(j,i,l+1,T_{av}(n)) - k_{eff}(j,i,l,T_{av}(n))] \end{aligned} \tag{4.9}$$

such that

$$\tau(j,i,p_{av}(n),T_{av}(n),u(n)) = \exp[-k(j,i,p_{av}(n),T_{av}(n)) \cdot u(n)] \tag{4.10}$$

In contrast to the implementation suggested by Kratz [16], the determination of the $k(j,i,p_{av}(n),T_{av}(n))$ for layers with average pressures that fall outside of the bounds of the 26 standard levels *are not* extrapolated from the nearest two $k_{eff}(j,i,l,T_{av}(n))$. Instead, only temperature fitting to determine the $k_{eff}(j,i,l,T_{av}(n))$ of the nearest standard level is performed. While the parameterizations described here share the same standard pressure levels employed by Kratz from 1000 mb to 0.251 mb, an additional 7 levels are used here. These additional standard levels extend the parameters to 0.01 mb, and allow interpolation for all but the highest possible layers. Above this height there is little pressure dependence to absorption line profiles, and the temperature fitting alone is sufficient. Likewise for any conceivable layers with $p_{av} > 1000$ mb, little additional pressure broadening from that at 1000 mb will be exhibited.

The second subprogram determines absorber-independent interval quantities. The first of these is the interval central wavelength, in μm, determined for the j^{th} subinterval as

$$\lambda_c(j) = \frac{1}{N}\sum_{i=1}^{N}\frac{10^4}{\nu(i)} \tag{4.11}$$

where N is the complete set of spectra occuring in all of the standard pressure levels composing the subinterval $\Delta g(j)$.

Interval parameterizations of source terms are also determined for solar and thermal sources. Both source types incorporate the ISR into the weighted averaging scheme. This is justified by considering the case of a spectrally dependent source reaching the instrument after passing through a path devoid of extinction processes. In this case, the instrument measurement will be the ISR weighted average of the spectral source. For shortwave bands, the interval-averaged TOA solar spectral flux, $\overline{F_0}(j)$, is determined from a reference data set that is cubic-spline interpolated to match k-spectra resolutions such that for the complete set of n spectral elements composing the j^{th} interval,

$$\overline{F_0}(j) = \frac{\sum_i^n F_0(\nu(i))\phi(i)}{\sum_i^n \phi(i)} \tag{4.12}$$

where the $\phi(i)$ are spectral ISR values that are also cubic-spline interpolated from calibration data, to match the k-spectra resolution.

In thermal spectral regions, interval Planck emission parameters are determined at 29 reference temperatures, T^B_{ref}, at a default 5 K resolution between 190K and 330K as

$$B(T^B_{ref}(l), j) = \frac{\sum_i^n B(T^B_{ref}(l), \nu(i))\phi(i)}{\sum_i^n \phi(i)} \tag{4.13}$$

where $B(T^B_{ref}(l), \nu(i))$ is the planck blackbody emission function for the l^{th} reference temperature at the i^{th} wavenumber in the j^{th} interval. This process serves to appropriately weight the source term contributions *within* the interval.

The interval Δg is defined in terms of the band-wide definitions, as

$$\Delta g(j) = \Pi_l(\Delta g(l)) \tag{4.14}$$

where $\Delta g(l)$ is the interval width at recursion level $1 \leq l \leq$ (number of absorbers in the band), serves as the primary interval results weighting term, which, as previously discussed, indicates the fraction of the band represented by the j^{th} subinterval.

The interval averaged ISR, is determined as

$$\overline{\phi}(j) = \frac{1}{n}\sum_{i=1}^{n} \phi(\nu(i)) \tag{4.15}$$

and serves as a second results weighting term. The set of $\overline{\phi}(j)/\sum\overline{\phi}$ indicate the relative sensitivity the instrument to the energy associated with each interval. When combined, the Δg and $\overline{\phi}$ terms, serve as 'instrument' interval results weighting terms, such that for some arbitrary radiative transfer calculation, $\mathcal{RT}$, the final result, $\mathcal{RT}_{final}$, is the compound interval width and ISR weighted sum of the N individual radiative transfer calculations, i.e.,

$$\mathcal{RT}_{final} = \frac{\sum_j^N \mathcal{RT}(j)\ \overline{\phi}(j)\ \Delta g(j)}{\sum_j^N \overline{\phi}(j)\ \Delta g(j)} \tag{4.16}$$

$\mathcal{RT}_{final}$ is then indicative of the results for the combined instrument-atmosphere radiative transfer system. In the following discussion of the validation of *.ck* parameters, such results are termed 'instrument' results, while those that do not include ISR are termed 'physical' results.

An additional pair of parameters, which measure the degree of correlation observed at the interval level are also determined. The first of these, p_1, is a metric of the average relative occurence of wavenumber intervals in *all* of the standard pressure levels, such that when p_1=1, every level is composed exactly the same set of wavenumbers, and when p_1=0, every level is composed of a unique set of wavenumbers. For the ℓ^{th} interval, p_1 is determined via a wavenumber interval 'AND'-ing masking operation as

$$p_1(\ell) = \frac{\sum_{\nu\in\ell} U(i)}{\sum_{\nu\in\ell} V(i)} \tag{4.17}$$

where $U(i) = 1$ if ν_i appears in every level, and 0 otherwise, and $V(i)$=1 if ν_i appears in any level, and 0 otherwise.

The second correlation coefficient, p_2, also measures average relative occurence of wavenumber intervals in all of the levels, but in a different sense. It seeks to determine, on average, in how many levels a given wavenumber composing an interval at some level appears. A value of p_2=1 implies that every wavenumber composing an interval occurs in every level, while p_2=0 implies that every wavenumber occurs in only 1 level. For the ℓ^{th} interval, p_2, is determined via a wavenumber interval 'OR'-ing and summing masking operation as

$$p_2(\ell) = \frac{\sum_{\nu\in\ell}\sum_j^{n_{levs}} W(i,j) - \sum_{\nu\in\ell} V(i)}{(n_{levs}-1)\sum_{\nu\in\ell} V(i)} \tag{4.18}$$

where $W(i,j) = 1$ if ν_i appears in the j^{th} level, and 0 otherwise. An error in the code to determine p_2 was recently found, so it will not be reffered to further.

These parameters are pulled together in the *.ck* file creation subprogram, which produces an ASCII file that can be read and used with appropriate code. It is independent of the number of absorbers present and separate radiative transfer calculations required. To date, code to read *.ck* files and determine interval parameters has been developed for the C and FORTRAN 90 programming languages. These codes, along with the currently released of collection *.ck* parameter files are available from the WWW site discussed in the first chapter.

4.4 Summary

In this chapter a means to create k-distribtution parameters for use in radiative transfer calculations was described. The process centers on a recursively invoked error minimization algorithm, which seeks to create Δg intervals producing transmission and relative absorption errors that are less than user-specified values for the range of optical paths likely to be encountered in the terrestrial atmosphere. A controlling program starts with the entire band, creates k-distributions for the strongest absorber, and calls the minimization program. When it successfully completes, the wavenumbers composing the first interval produced are then used and the process continues until all of the absorbers and intervals are minimized. The controlling program then calls another program to create the *.ck* parameters file, containing all of the information necessary for radiative transfer calculations.

Chapter 5

MAS k-Parameters: Validation Results and Discussion of Errors

The error minimization scheme discussed in the last chapter was applied to the 50 MAS channels during the Fall 1997 term. The large number of channels involved made this a time consuming process, and took nearly a month to complete. However, the relatively wide portion of the electromagnetic spectrum and spectral features that were parameterized during the course of this effort proved to be a valuable application of the development process. Nearly all of the types of overlapping aborption (e.g. weak-weak, weak-strong, strong-strong, etc.) were encountered in the MAS channels. The interaction of these absorption features with sources ranging from the strongest part of the solar spectrum through much of the thermal spectrum permitted a determination of the efficacy of the parameterization process in the general sense, and helped to bring about an understanding of circumstances where a 'perfect' parameterization of absorption (contradictory as that may seem) may be insufficient to permit the accurate description of band radiative transfer.

In this chapter, the description of a procedure that seeks to validate the k-parameters and the results of these validations are presented. It is shown, at least for the profile employed, that the parameters produced for the 50 MAS bands are sufficiently accurate to permit their use in retrieval applications, in that the discrepancies between $.ck$ and LBL results for every channel are within measurement errors likely to be encountered, and in many cases are smaller than the detector sensitivities. The fact that any non-negligible errors exist required some analysis. The results of an investigation seeking to determine

the relative importance of the factors giving rise to the exhibited errors is presented, and the need for an additional constraint, which will be employed in future applications of the parameters development system, is discussed.

5.1 Validation Procedure and Results

Though the minimization process ensures that the interval absorption coefficients are valid over the range of paths likely to be encountered in the modeling of the terrestrial atmosphere, it is impossible to know *a priori* whether or not the results obtained with the complete set of parameters will be sufficiently accurate. In order to identify cases where refinements to the *.ck* paramters are required, a validation procedure which measures several aspects of the results obtained with their use was adopted. The procedure makes use of a *plane-parallel, adding-doubling* radiative transfer model[1], developed jointly by C.J. Drummond and S.D. Miller. This model, which is capable of performing single-line, band line-by-line, and band k-parameter calculations, allows the user to choose from a wide range of profile options, including the specification of standard atmospheric profiles, variations on a set of standard aerosol profiles, and clouds with arbitrary physical and/or optical parameters.

A test case, using a modified McClatchey Mid-Latitude Summer (MLS) profile under clear-sky conditions devoid of aerosols is employed in a pair of line-by-line and k-parameters calculations. Considering the results from the line-by-line calculation to be exact, the k-parameters results are compared to determine how well they match. Immediately after the *.ck* file is created, this validation procedure is performed by the k-parameters creation controlling program.

A typical example of the results of this validation procedure are shown in Figure 5.1. Plots of 'instrument' layer heating rates, 'instrument' upwelling near-nadir level radiances, layer band-averaged 'physical' gaseous optical depths and the 'instrument' downwelling

---

[1]See, e.g. Stephens and Greenwald [13], Goody and Yung [12] for details of the adding-doubling approach.

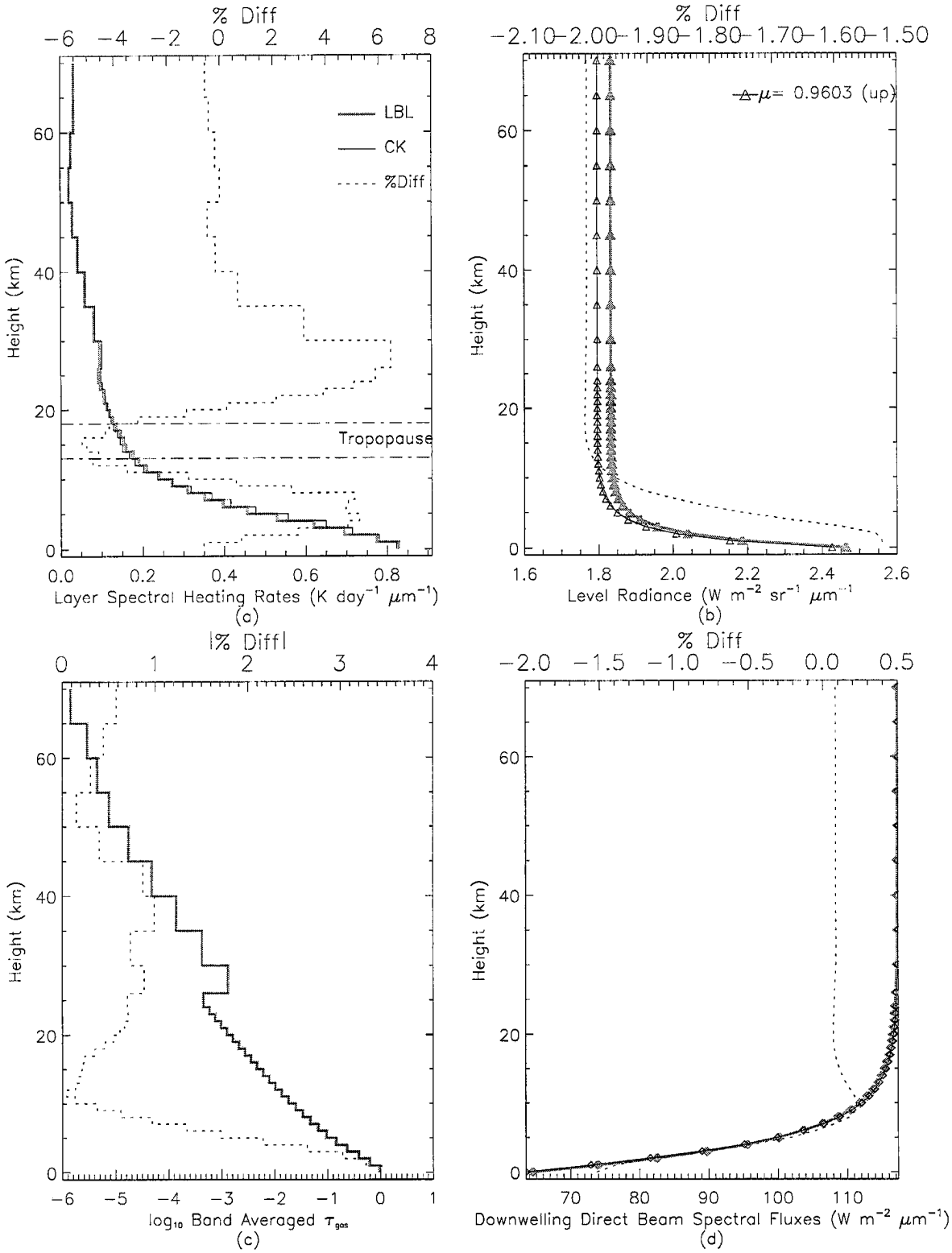

Figure 5.1: MLS Profile validation results for MAS Channel 17. (a). 'Instrument' layer heating rates, (b). 'Instrument' level near-nadir upwelling radiances, (c). 'Physical' layer band-averaged gaseous optical depths, and (d). 'Instrument' downwelling direct beam spectral fluxes.

direct beam spectral fluxes are shown, each containing comparisons of line-by-line and *.ck* parameters and the % differences between them at each layer or level in the atmosphere. All of the results, except for the optical depths, employ model results that include the effects of the ISR on measurements, and as such are 'instrument' as opposed to true physical values.

These plots served to reveal several aspects of how well the *.ck* parameters worked. The heating rate plots, which employ layer flux divergences, are not particularly useful in remote sensing applications, but serve as an indication of how well the *.ck* parameters serve to represent the radiative transfer within the band and depth of the atmosphere as a whole. This metric alone is insufficient, as only the differences in intensities are involved, such that a *.ck* parameters set with gross systematic biases in layer optical depths might produce satisfactory heating rate results. The upwelling near-nadir radiances serve to resolve this factor and are a primary determinant of the efficacy of *.ck* parameters set. The plot of band averaged layer optical depths serves to isolate the validity of the ensemble of k_{eff} parameters employed in the test profile, though the layer average values are typically dominated by the influence of the strongest absorption lines and intervals. For shortwave channels, such as the one shown in Figure 5.1, an additional plot comparing the intensity of the downwelling solar spectral flux at each level was produced. At the top of the profile, the values indicate how well the set of interval $\overline{F_0}$ parameters match the spectral solar flux across the band, while through the depth of the atmosphere and especially at surface, they indicate how well the combination of interval $\overline{F_0}$ and k_{eff} parameters represent the attenuation of the direct beam alone, thus eliminating the effects of multiple scattering. The direct beam values include the effects of extinction due to Rayleigh scattering, but since such scattering is a slowly varying quantity in spectral space, and the MAS bands are relatively narrow, it effectively only acts as a constant added to the layer gaseous optical depths in each interval.

While some disagreement between the results of the two calculations is inevitable, the degree of these errors through the depth of the atmosphere, relative to the expected errors associated with instrument measurements serve as the determining factors in the decision

whether or not to accept the *.ck* parameters as 'valid.' Some error is inherent in all experimental measurements, and while calibration procedures seek to reduce any systematic biases, engineering considerations dictate limited instrument sensitivity. The existance of random measurement errors also compromise the fidelity of instrument measurements. A recent paper by King, *et al* [14], includes indications of channel sensitivities, as a set of Channel Equivalent Noise parameters, in terms of radiances for shortwave channels and brightness temperatures for longwave channels. A source involved with the management of the MAS instrument indicated that these numbers refer to detector sensitivities and are therefore a lower bound on the measurement errors that can be expected. More generally, a error of up to 5% of the measured radiance can be expected when calibration errors are taken into account. As such, a parameterization which produces test-case errors within these bounds was considered acceptably valid, since there is no point in wasting CPU cycles in extra interval calculations in order to produce results that are more accurate than the measured radiances. When *.ck* parameters results for a channel were much more accurate than the indicated instrument noise, if a large number of calculations were required, the k-parameters creation process was re-run with a looser set of minimization criteria. Conversely, when the validation procedure revealed radiance errors greater than the 5% upper bound, the creation process was re-run with steps to improve the results.

A summary of the validations results for each of the 50 MAS channels, along with the number of *.ck* intervals, the channel $\overline{p}_1$ level correlation coefficient, which is determined as the interval-width weighted average of the interval p_1 values, and Instrument Equivalent Noise values are shown in Tables 5.1 and 5.2.

The shortwave channel results comparisons in Table 5.1 are in terms of the TOA near-nadir radiances determined directly from LBL and *.ck* calculation quadrature angles. In the 8-stream calculations employing a Gaussian angular quadrature scheme, this corresponded to a viewing angle approximately 16^o off nadir, which while somewhat arbitrary, eliminates any additional errors that may be introduced by extrapolating the results at quadrature points to aboslute nadir. Most of the results indicate differences between the two apporaches that are less than 2% of the LBL radiances, well below the 5% error

Channel	λ_c (μm)	Inst. Noise	.ck Params		MLS Profile Validation Results	
			No.Intervals	$\overline{p_1}$	$\Delta I(\text{TOA}^{\uparrow})$	%Diff$\lvert(\Delta I)\rvert$
1	0.541	0.3350	1	1.0000	1.39331	1.61
2	0.644	0.1570	5	0.9848	0.93936	1.42
3	0.695	0.1780	12	0.7881	0.26779	0.50
4	0.736	0.1800	12	0.7312	0.90631	2.01
5	0.776	0.2540	8	0.9633	-0.04377	0.10
6	0.817	0.2370	6	0.7104	1.33227	3.59
7	0.860	0.2810	10	0.8224	0.03652	0.10
8	0.899	0.1500	17	0.6954	0.60425	2.12
9	0.941	0.2260	9	0.4501	0.50442	3.79
10	1.642	0.0390	4	0.9081	-0.08014	0.92
11	1.696	0.0290	5	0.8689	0.04514	0.60
12	1.751	0.0260	7	0.7203	-0.05918	1.17
13	1.803	0.0260	10	0.6276	0.03739	4.26
14	1.855	0.0250	10	0.5830	-0.00057	8.60
15	1.904	0.0290	32	0.4340	-0.00110	12.78
16	1.973	0.0140	55	0.3307	-0.03034	4.27
17	2.005	0.0190	44	0.3526	-0.03664	2.00
18	2.054	0.0220	35	0.6312	-0.00667	0.25
19	2.100	0.0120	27	0.5248	-0.10597	3.40
20	2.151	0.0030	4	0.8641	-0.04130	1.46
21	2.198	0.0230	4	0.8968	0.01432	0.57
22	2.249	0.0260	4	0.9492	-0.04007	1.59
23	2.298	0.0270	6	0.9196	-0.05046	2.41
24	2.344	0.0260	7	0.7725	0.00720	0.46
25	2.390	0.0330	8	0.7582	-0.01408	1.33

Table 5.1: MAS Shortwave Channel *.ck* File Parameters and Validation results. Instrument Noise Values (source: King, *et al* [?]) and $\Delta I(\text{TOA}^{\uparrow})$ are in terms of radiances ($Wm^{-2}sr^{-1}\mu m^{-1}$).

threshold and are thus deemed unconditionally acceptable. Of the 9 channels where the errors are larger than 2% of the LBL radiances, 7 of them exhibit errors less than 5%, and 2 of these have errors near to or less than the specified instrument noise values. The 2 channels with errors greater than 2% are well within the instrument noise values. This leaves 5 channels with relative errors between 2% and 5%, that in absolute terms are in excess of the channel's rated instrument noise values. While still considered valid, some of these channels will be discussed in more detail in the discussion of error sources, below.

Of the 25 longwave channels results in Table 5.2, 17 exhibit radiance errors that are less than 2% of the LBL results. Of these 17, the errors associated with 14 are also less

MAS Channel	λ_c (μm)	Inst. Noise	.ck Params		MLS Profile Validation Results		
			No.Ints.	$\overline{p_1}$	$\Delta T_B(\text{TOA}^{\uparrow})$	$\Delta I(\text{TOA}^{\uparrow})$	%Diff$\lvert(\Delta I)\rvert$
26	2.846	9.7800	81	0.4139	-4.67599	-0.00374	25.21
27	3.012	7.0500	35	0.4550	-0.18928	-0.00076	0.96
28	3.182	3.0900	48	0.5302	-3.59326	-0.02496	15.86
29	3.346	1.2800	41	0.5077	0.17925	0.00202	0.81
30	3.510	0.7200	39	0.6369	-0.31093	-0.00769	1.23
31	3.660	0.4700	3	0.9808	-0.17157	-0.00494	0.67
32	3.821	0.3700	4	0.8387	-0.26512	-0.00810	1.03
33	3.976	0.3000	1	1.0000	-0.08626	-0.00287	0.33
34	4.130	0.8100	8	0.8784	0.64327	0.01173	2.87
35	4.279	1.7400	25	0.4744	0.97503	0.00456	5.70
36	4.440	0.2800	41	0.3172	0.95097	0.01853	4.29
37	4.604	0.1400	69	0.1769	-1.24697	-0.04916	4.66
38	4.750	0.1300	91	0.1723	0.20840	0.00959	0.77
39	4.922	0.1200	76	0.3068	-0.41615	-0.02134	1.49
40	5.069	0.1400	11	0.7690	-0.81260	-0.04262	2.88
41	5.215	0.1800	8	0.8268	-0.50992	-0.02303	1.89
42	8.505	0.1400	13	0.7773	0.09764	0.01552	0.20
43	9.663	0.1200	52	0.1009	2.08859	0.25308	4.29
44	10.516	0.0900	8	0.7475	-0.01298	-0.00183	0.02
45	11.014	0.1000	5	0.9145	-0.06514	-0.00865	0.10
46	12.014	0.1900	6	0.9096	-0.18657	-0.02143	0.27
47	12.787	0.4600	15	0.7500	-0.33441	-0.03347	0.46
48	13.284	0.4900	29	0.5388	-0.05146	-0.00448	0.07
49	13.773	1.3200	34	0.4231	0.43011	0.03035	0.67
50	14.270	2.0000	42	0.4063	-0.58374	-0.03132	1.04

Table 5.2: MAS Thermal Channel *.ck* File Parameters and Validation results. Instrument Noise Values (source King, *et al* [?]) and $\Delta T_B(\text{TOA}^{\uparrow})$ are in terms of brightness temperatures (K).

than the instrument noise, expressed in terms of brightness temperatures. Five channels have relative radiance errors between 2% and 5% of LBL values, 4 of which are greater than the instrument noise values. Two channels (26 and 35) which have large relative radiance errors that, while also indicative of non-negligible brightness temperature errors, are also well within instrument noise values. While the results for these two channels are 'acceptable', the combination of instrument noise and *.ck* parameters errors preclude their further use. This leaves only channel 28, with a large relative radiance error that translates as a brightness temperature error greater than the instrument noise value. This channel is also examined in the discussion of error sources, below.

Overall, the results indicate that the *.ck* parameters creation process developed in this study produces acceptable results when applied to a realistic atmospheric profile. While the parameters are only applied to a single profile, given the way that they are employed and that the test involved their application to an atmosphere with greater vertical resolution than the parameters themselves, there is little reason to expect that comparisons employing other profiles would dramatically differ from those found in this test.

5.2 Sources of Errors in *.ck* Parameters

Since 'errors' were found in the test case, it is worthwhile to attempt an examination of how they arise. Upon consideration of how the *.ck* parameters are used to represent radiative transfer in the bands, 3 or 4 possible sources arise, which are presented and discussed separately in the following paragraphs. It is *not* a simple task to identify the degree to which any of the possible error sources are contributing to the errors observed in the validation runs. In fact, since the calculated radiances are the result of interactions involving multiple scattering between all layers, it appears impossible to identify specific error contributions, and simplifying or oblique approaches to their import are taken.

The first of these types of error sources may arise from 'bugs' in the nearly 28,000 lines of IDL code used in their creation. A not insignificant portion of the effort in developing this application involved testing and validating the individual function and subroutines composing the application. Many of these procedures were relatively straightforward to debug, since a rigorously modular approach was taken in the system design. This approach ensured that once a particular procedure was sufficiently tested, its results were reliable in any subsequent application. The development of the recursive minimization process, which was probably the single most complicated part of the project, involved the creation of code to perform wavenumber interval tracking between recursion levels, and required the most extensive testing and debugging. The testing procedures in this phase involved both numerical and graphical comparisons of the subsets of band spectra passed from level to level, as well as tests of the resultant parameters to ensure that each wavenumber

interval in the band appeared once and only once in each of all of the standard pressure level k-distributions, and that the k_{eff} parameters accurately represented the wavenumber intervals from which they were determined. While it can not be unequivocally stated that the application is devoid of *any* bugs, the absence of any truly gross disagreements between LBL and *.ck* results, and the confidence gained from the extensive testing procedures employed, permit the statement that any possible bugs in the system are inconsequential.

5.2.1 Anti-Correlations

The existance of anti-correlations between the k-distribution intervals at standard pressure levels, examples of which were shown in Figure 3.2, have been identified (West, *et al*, [32]) as *the* cause of the breakdown of Correlated-k approaches. When significant anti-correlation of the wavenumbers composing a Δg interval in different layers of the atmospheric profile occurs, the radiative transfer process is effectively considering different subsets of the band at different layers. At the high g-space resolution shown in Figure 3.2 it is easy to see that this will lead to the 'disappearance' of photons associated with absorption coefficients as they propagate across layer boundaries, and their replacement by a different set. The relatively wide Δg intervals employed in the k-parameters, however, largely mitigate these effects since relatively wide spectral sub-bands are included in each interval and only those photons not associated with *every* layer's k_{eff} are potentially problematic. The source term weighting scheme described in §4.3 compensates for these effects in applications where the profile being modelled is similar to the set of standard pressure levels, but may lead to inaccuracies in the source terms in highly anti-correlated intervals where only a few standard pressure levels are referenced. Thus, anti-correlations may give rise to two distinctly different error components in each interval calculation: those resulting from poorly parameterized sources, and those resulting from absorption coefficients representing different spectral regions through the depth of the atmosphere. The first component decreases the validity of source term parameters in any profile, while the second acts in a profile dependent way to skew the absorption and scattering characteristics of incident and emitted radiation. The importance of these contributions to errors is difficult to determine, in that in order to be observed, a multi-layered inhomgeneous

atmosphere is required, and the matrix of radiance contributions from all layers at each layer boundary must be identified.

Instead of attempting to analyze the effect of anti-correlations at this level of detail, a less tedious approach was taken. By comparing the first correlation parameter, $\overline{p_1}$, associated with each *.ck* parameters set and the MLS profile validation %Diff$|\Delta I(\mathrm{TOA}^{\uparrow})|$ values from Tables 5.1 and 5.2, some insight on the effects of band-wide anti-correlations can be gained. As shown in Figure 5.2, where the results for the 45 channels with errors less than 5% are plotted against their corresponding $\overline{p_1}$ values, it is not clear that anti-correlations are primarily responsible for the errors exhibited. This is obviously not an ideal comparison, since in addition to being dependent on the particulars of how the standard pressure level parameters are implemented, the % difference statistic alone does not indicate whether the errors are significant with regard to expected instrument measurement errors. Considering this comparison as indicative of the role of anti-correlations in the MLS profile results alone, it is, however, clear that while there is perhaps some correlation[2] between $\overline{p_1}$ and %Diff$|\Delta I(\mathrm{TOA}^{\uparrow})|$, anti-correlations, if they do contribute to errors at all, are not the only or even the primary source of errors. The correlation statistics developed in this study would then seem to refute the assertion that anti-correlations are alone responsible for the breakdown of Correlated k approaches.

5.2.2 Interpolation Errors

Another source of error that is inherent to the *.ck* parameterizations arises from the inability of the interpolation of discrete standard pressure and polynomial-fit temperature k_{eff} parameters to accurately reflect the character of absorption in profile layers with arbitrary average pressures and temperatures. Such errors in the k_{eff} will arise : a) when the changes in line broadening with pressure are not sufficiently resolved by $\Delta \log_{10} p$ standard level spacing and/or b) when the changes in line strength and line broadening with

---

[2]For the sample of 45 channels plotted in Figure 5.2, the linear Pearson correlation coefficient, ρ, between $\overline{p_1}$ and %Diff$|\Delta I(\mathrm{TOA}^{\uparrow})|$ is -0.48224. Including the other 5 channels with larger %Diff$|\Delta I(\mathrm{TOA}^{\uparrow})|$ values, ρ drops to -0.35772.

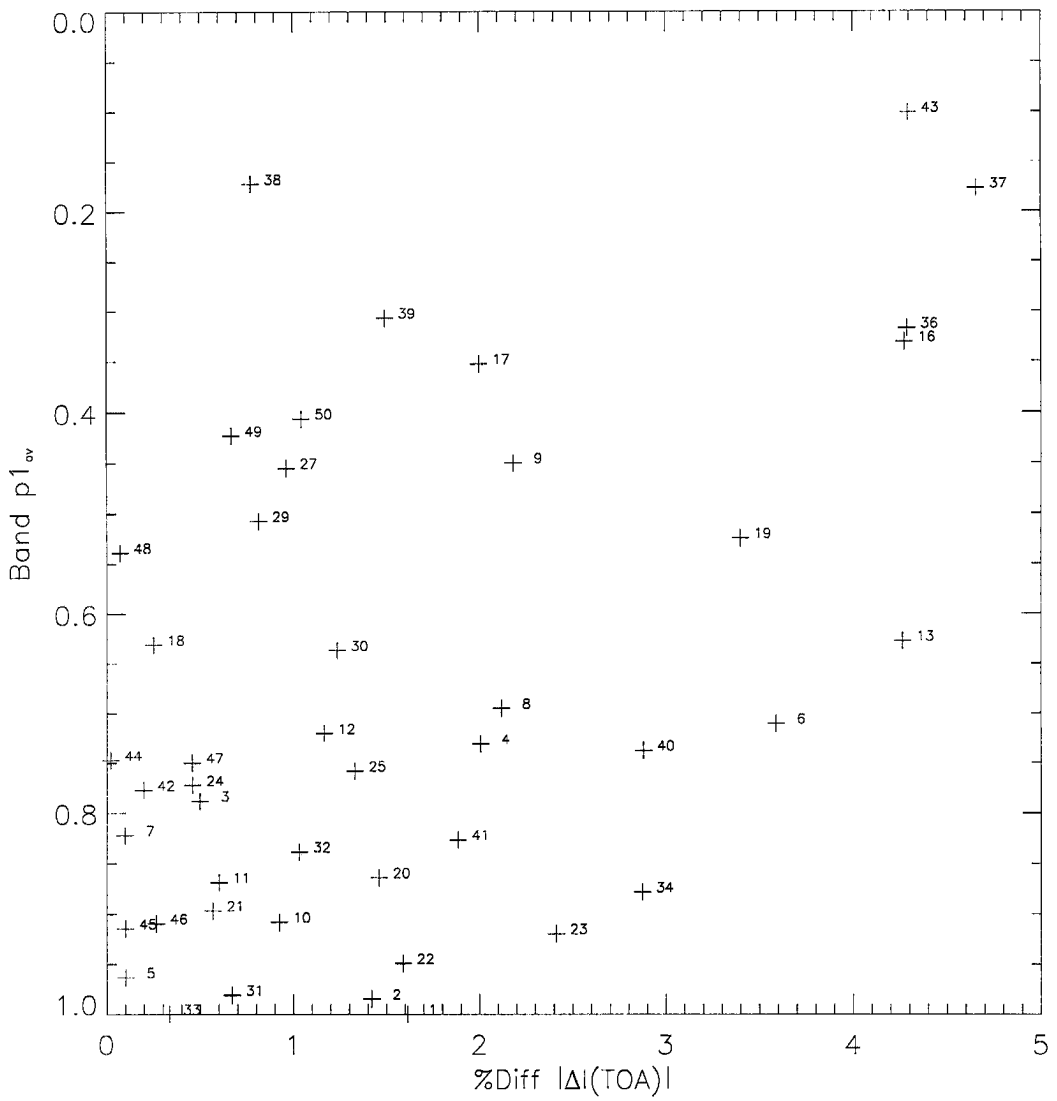

Figure 5.2: Comparison of MAS band correlation statistics and MLS validation profile %Diff$|\Delta I(\mathrm{TOA}^{\uparrow})|$. The numbers next to the crosses indicate the MAS channel associated with the ($\overline{p_1}$, [%Diff$|\Delta I(\mathrm{TOA}^{\uparrow})|$]) pair.

temperature are poorly fit by the quadratic polynomial in temperature. The magnitude of such errors and their contribution to errors in optical depths are entirely dependent on the profile being employed. This being the case, a rigorous analysis of their potential affects on each of the 50 sets of *.ck* parameters was not feasible. During the parameters validation process, one of the factors considered in deciding whether or not to accept a *.ck* parameters set were the errors in the band-averaged layer optical depths and heating rates. Generally these appeared to be relatively minor (on the order of a few percent for column optical depths), though instances of layer heating rate errors as large as 25% were found. This suggests that while not completely negligible, in general interval-layer interpolation errors alone will not substantially contribute to the errors exhibited in arbitrary profiles.

5.2.3 Source-Absorption Coupling

In certain bands it was found that although the band-averaged layer optical depths were quite well represented by the *.ck* parameters, relatively large TOA radiance errors occurred. This was initially a source of frustration as repeated interval error minimizations with progressively stricter minimization criteria seemed to only have the effect of increasing the number of interval calculations required, without significantly improving the results obtained. Upon consideration of the limitations of band models, as discussed in §3.2, the possibility emerged that the interval-averaged source and absorption parameters, though individually valid, when employed in conjunction with each other produced non-negligible errors as the details of the spectral combinations of each were lost. Consider, for example, the band averaged attenuation of the direct solar flux through the depth of the atmosphere. In LBL calculations the 'instrument' direct beam reaching the surface, which includes the ISR as a spectral weight, will be determined as

$$\begin{aligned} F_{sfc}(LBL) &= \frac{\sum F_0(\nu)\exp(-\tau_\nu^*)\phi(\nu)\Delta\nu}{\sum \phi(\nu)\Delta\nu} \\ &= \overline{F_0 T} \end{aligned} \tag{5.1}$$

where the τ_ν^* is the column optical depth including the effects of gaseous absorption and rayleigh scattering. The *.ck* equivalent will be determined as

$$F_{sfc}(CK) = \frac{\sum \overline{F_0}(i)\exp(-\tau_i^*)\overline{\phi}(i)\Delta g(i)}{\sum \overline{\phi}(i)\Delta g(i)}$$

$$= \overline{F_0} \cdot \overline{T} \tag{5.2}$$

To the degree that there is significant variability in these spectrally coupled $F_0 \cdot T$ values, disagreements between the two forms of F_{sfc} will result. This is analogous to (though not precisely) the definition of variance, and is an indication of how closely a member of a sample will correspond to the sample mean. Conversely, if either F_0 or T are spectrally flat in regions where $\phi \gg 0$, the two forms will be equivalent. This type of error can be especially problematic in conventional CKD approaches where spectral mixing occurs at band-wide level and only band-averaged source terms can be employed. In the implementation developed in this study, the isolation of spectral absorption and source contributions at the Δg interval level should largely mitigate such effects, since the spectral range in transmission being determined from a single τ^* value is limited by the recursive approach. Instances where it does occur can be identified by comparing the validation plots of band-averaged optical depths and and TOA radiances or surface downwelling fluxes, where available.

Two cases where coupling errors may be the significant source of disagreements between *.ck* and LBL results occur in channels 9 and 28, both of which showed marginal validity. Relevant band-averaged LBL and *.ck* calculation results are shown in Table 5.3. Channel 9 is centered on the 0.94 μm water vapor absorption band. The band averaged column optical depths differ by only about 1/10th of 1%, but the differences in the direct beams reaching the surface differ by nearly 3.7%. Further, while the *.ck* parameters produce a larger column optical depth, they also result in a stronger direct beam surface flux which indicates that spectral coupling contributes an error at least as large as that observed in F_{sfc} values. The results for Channel 28, centered near 3.18 μm are also dominated by strong water vapor absorption, but also include spectrally distinct overlapping weak absorption by CH_4, O_3, and N_2O. In this channel, while the *.ck* band-averaged column optical is slightly smaller than the LBL result, the surface direct beam flux is also smaller. It is interesting to note that for both of these channels, the $\%\text{Diff}|\Delta I(\text{TOA}^{\uparrow})|$ errors are nearly the same as the errors in the downwelling direct beam at the surface, which indicates that the k_{eff} parameters are sufficiently accurate. Thus, spectral coupling can be an important contribution to errors in *.ck* parameters.

Chan	$F_0(LBL)$	τ^*_{lbl}	τ^*_{ck}	%Diff(τ^*)	$F_{sfc}(LBL)$	$F_{sfc}(CK)$	%Diff(F_{sfc})
9	813.522	2.2052	2.2078	-0.11681	432.514	448.483	-3.69222
28	20.0041	16.803	16.735	0.06816	5.06926	4.42672	15.9694

Table 5.3: MAS Channels 9 and 28 LBL, *.ck* coupling error contributions. In both cases, the relation of the column optical depths are of the same sign as the relation of the surface fluxes, which indicate that spectral coupling of source and absorption terms is a relevant factor to consider.

Results such as those found for Channels 9 and 28 indicate that an additional constraint in the development of *.ck* parameters might be employed. In correspondening with several authors of papers concerned with CKD applications, all indicated that they had not considered the role of source-absorption coupling in their studies, and no references were found to it in the relevant literature. This additional constraint is thus probably a new consideration, which will help improve the validity of k-parameters. In remote sensing applications, it will allow for the segregation of physically distinct source-absorption strengths, from which separate k-distributions might be developed. In radiation scheme applications, such as in GCMs, it will help to better define separate bands over which to do radiation calculations, and improve the fidelity of intra-band calculations.

5.3 Summary

In this chapter, a procedure to validate *.ck* parameters created with the system developed in this study is described, the results of the validation of the MAS parameters is shown, and the factors contributing to observed disagreements between line-by-line and *.ck* calculations are discussed. It was found that while some disagreements between the two calculation approaches invariably exist, in most cases the errors associated with the *.ck* parameters are less than those that can be expected from instrument measurements. This result indicates that the *.ck* parameters creation process that was developed in this study is generally valid and is thus applicable to a wide range of overlapping absorption bands across the solar and thermal spectral regions.

In those cases where significant disagreements between the validation results were observed, it was found that the spectral coupling between absorption coefficients and source

terms is perhaps the most important source of error. This is in contrast to previous studies, which have assumed that anti-correlations between the k-distributions at standard pressure levels are the primary cause of the breakdown of conventional CKD approaches. The k-parameters creation process serves to segregate spectrally distinct absorption coefficients into Δg intervals within which the k_{eff} values reasonably approximate the range of observed absorption. The identification of spectral coupling as a potential source of error permits the development of a diagnostic to identify, and thus remedy, spectral subsets of Δg intervals within which coupled source-absorption terms are distinct enough to lead to significant errors. Though not treated in the parameters created for the sometimes noisy MAS channels, the validity of parameter sets developed for more precise instruments and bands where higher fidelity between spectral and k-parameters calculations are required, will be improved by this analysis technique.

Chapter 6

Summary and Conclusions

An accurate and computationally efficient means to describe the effects of gaseous absorption on radiative transfer in the terrestrial atmosphere is a necessary prerequisite to the development of a method which seeks to characterize upper tropospheric cloud and water vapor properties from radiometer measurements. The development of a valid procedure to retrieve these properties from measurements made by the MODIS instrument, which is scheduled for launch aboard the EOS AM-1 platform in 1998, is the eventual goal of this researcher. In the interim before MODIS data become availible, measurements collected during the 1996 SUCCESS field experiment by the 50 channel MAS instrument, which is similar in many aspects to MODIS, are to serve as the basis for the development of a MODIS 'Observing System'.

The long established 'Correlated k-distribution' approach appeared to be the most feasible route to the objective of characterizing gaseous absorption, though the paucity of available parameter sets for the 50 MAS Channels, along with the impression that this would remain the case, required the development of a system to independently produce them. During the course of the development of this system, an alternative to conventional approaches to the creation of k-distribution parameters emerged and was pursued. A novel procedure to create k-parameters that is broadly applicable in forward radiative transfer modeling was thus developed. The parameter sets that can be created with this approach retain significant spectral information and isolate the effects of overlapping absorption features at the calculation interval level. An important component of these parameters is the inclusion of the effects of spectrally varying instrument response on

resultant instrument radiance measurements. The parameters sets developed in this study have been demonstrated to be adequately valid for most of the 50 MAS channels in the visible through infra-red spectrums. This being the case, a significant first step toward the creation of a MAS 'Observing System' of upper tropospheric properties has been accomplished.

Parameter sets were created from high resolution synthetic absorption coefficient spectra. These k-spectra were created for each of the relevant absorbers in a band at 26 standard pressure levels and 3 standard temperatures via the superpostion of Voigt profile broadening contributions of transition lines appearing in the HITRAN atlas. A recursively invoked transmission and relative absorption errors minimization scheme, which produces k-distribution intervals meeting user specified error criteria, serves as the core of the parameters creation system. It employs subsets of the band spectra that are determined from 'higher level' minimization results to create interval-specific k-distributions. These k-distributions are then used in conjunction with standard pressure level specific ranges in optical paths to determine Δg space intervals which are valid for the range of absorber amounts that can be expected in the terrestrial atmosphere. This novel process, in conjunction with the accounting of the spectral-space components of each Δg interval, allows the determination of ancillary interval-specific parameters which, in addition to interval-averaged ISR information, include more accurate parameterizations of source terms than are possible with conventional approaches.

A validation procedure which compares several aspects of the results obtained with the parameters developed in this study against those obtained with line-by-line calculations indicated that the *.ck* parameters created are valid. For most of the MAS channels, it was found that the disagreements between the results of these two approaches were less than the errors that might be expected in instrument measurements themselves. The parameter sets for a few of the MAS channels produced relatively large errors. An examination of the sources of the errors in these channels revealed that while the role of anti-correlations can not be ruled out, it appears that discrepancies arising from the treatment of spectrally coupled source and absorption quantities as single valued means in intervals with significant variance in either of these terms is the primary source of errors. The identification

of this error source permits the development of a diagnostic to alleviate its effects via the segregation of spectral components with similar source terms. While not applied to the MAS parameters developed here, the identification of errors arising from the treatement of spectrally coupled absorption and source terms as single-valued means in Δg intervals has the potential to further increase the fidelity of subsequent k-parameters creation efforts.

6.1 Summary

There are numerous particular conclusions to be drawn from this study, that would be tedious to reiterate in detail yet again. However, the most important conclusions, representing the more significant aspects of the results of this study can be summarized as follows:

- The novel approach to k-distribution parameters creation developed in this study permit an accurate and computationally efficient description of the effects of gaseous absorption on radiative transfer in the terrestrial atmosphere and the modelling of instrument-measured radiances.

- The relative absorption and transmission errors minimization scheme used to create k-distribution parameters is sufficient to adequately describe the optical depth contributions resulting from absorption processes in the terrestrial atmosphere.

- Spectrally varying source term and absorption coefficient coupling within specific k-parameters calculation intervals can be an important source of errors. Since the variance of the spectral components of interval k_{eff} parameters are limited by the creation process, the identification and alleviation of significant variance in interval source term components will potentially further improve the fidelity of subsequent k-parameters creation efforts.

6.2 Future Work

The next step in this investigation is the development an 'Observing System' from an ensemble of MAS channels containing information useful to the retrieval of upper tropospheric cloud and water vapor properties. The tenuous nature of our understanding of

ice cloud scattering properties makes this an ambitious objective. It remains to be determined what, if any, of these parameters can be reliably retrieved from MAS radiances, though the k-distribution parameters developed in this study provide a wealth of potentially useful information. Several ER-2 flight legs from the SUCCESS mission have been identified in which cirrus clouds were observed by MAS and LIDAR instruments. Given positive indications of observing system capabilities, it is planned to use the k-parameters developed in this study as a component of demonstration retrievals from MAS, and if possible, equivalent MODIS channel radiances.

Appendix A

.ck Parameters File Structure

This appendix describes the *.ck* file structure associated with each of the k-distribution parameter sets produced in this study. For the MAS instrument, the files are named 'mas##.ck', where '##' represents the two-digit channel number. The files are stored in ASCII format, with variable record lengths determined by individual field sizes and the number of fields in each record. The files are broken into three categories of record types and occur in the following order within the files:

- IC (File Header Records) : One set of records per file.
- RS (Recursion Structure Definition Record) : One record for each absorber included in the file.
- CK (CK Data Records) : One set of records for each calculation interval.

The definitions for each of the types of records are as follows:

Rec	Field	Type/Size	Field Name	Description
IC0	0	char[80]	Comment-0	File description 0
IC1	0	char[80]	Comment-1	File description 1
IC2	0	int	instrument_no	Reference Instrument #
	1	int	channel_no	Channel Instrument #
IC3	0	double	lambda0	Band begining wavelength (μm)
	1	double	lambda1	Band ending wavelength (μm)
	2	double	lambda_c	Band central wavelength (μm)
	3	double	dlambda	Band width (μm)
IC4	0	int	n_absorbers	# of absorbers parameterized
	1	int	n_calcs	# of radiative transfer calcs required
	2	int	n_ck_recs	# of CK parameterization records (same as n_calcs in this rev.)
IC5	0-2	double[3]	cf_temps	the set of i=[0,1,2] temperatures used in developing the CK parameterizations. cf_temps[1] is base temperature from which correction factors to level abs. coefficients are based (250K)
IC6	0	int	n_std_levs	# of reference levels for which abs. coefficients are defined (at the base temperature).
	1-	double[]	std_levs	the reference pressure levels at which the interval k-coeffs are defined. (mb)
IC7	0	int	n_B_temps	# of interval Planck emission temperatures
	1	double	B_t0	the first Planck emission temp. (K)
	2	double	B_t1	the last Planck emission temp. (K)
	3	double	B_dt	the increment between Planck emission temperatures (K)

Table A.1: File Header (IC) Records

Rec	Field	Type/Size	Field Name	Description
RS0	0	char		50 char '=' rec seperator
RS1	0	int	level	params creation recursion lev / absorber index #
	1	int	ht_absorber_id	HiTran absorber # (e.g. 1=H2O, 2=CO2, 3=O3, ...)

Table A.2: Recursion Structure Definition (RS) Records

Rec	Field	Type/Size	Field Name	Description
CK0	0	char		50 char '-' rec seperator
CK1	0	int	set_no	CK data record set #
CK2	0	string	uniq_id	InstChan.Uniq subinterval ID string
CK3	0-	int[]	subint_id	array of size 'level' containing the unique set of subinterval identifiers (a sanity check)
CK4	0	double	int_filter_av	subinterval avg'd instrument filter function
	1	double	int_dg	subinterval cum. k-dist. width
	2	double	int_lambda_c	subinterval avg'd central wavelength (μm)
	3	double	int_Ida0	subinterval avg'd TOA solar spectral flux ($Wm^{-2}\mu m^{-1}$)
	4	double	int_p1	subinterval creation wavenumber total correlation (p_1) statistic
	5	double	int_p2	subinterval creation wavenumber partial correlation (p_2) statistic
CK5	0-	double[]	int_B	array of size [n_B_temps] containing subinterval Planck black body emission radiances for use in interpolating layer emissions.($Wm^{-2}sr^{-1}\mu m^{-1}$) (Newlines are inserted after every n_B_temps entries.) Note: valid for B_temps[0] $\leq$ T $\leq$ B_temps[n_B_temps-1]. (Source is the averaged emissions for the wavenumber intervals sets in the T=250K k-distributions)
CK6	0-	double[][]	int_lev_k	array of size [n_absorbers][n_std_levs] containing the k-coeffs for each absorber @ T = 250 K. (Newlines are inserted after each n_std_levs entries.)
CK7	0-	double[][][]	int_lev_Tc_coef	array of size 'n_absorbers,3,n_std_levs' containing quadratic polynomial coefficients to fit a k-coeff to (T-250). (Newlines are inserted after every n_std_levs entires.)

Table A.3: CK Data Records

Bibliography

[1] T.P. Ackerman, 1979. On the effect of CO_2 on atmospheric heating rates. *Tellus*, **31**, 115-123.

[2] V. Ambartzumian, 1936. The effect of the absorption lines on the radiative equilibrium of the outer layers of the stars. *Pupl. Obs. Astron. Univ. Lenningrad*, **6**, 7-18.

[3] C.N. Banwell: *Fundamentals of Molecular Spectroscopy, 3rd Ed.* (McGraw-Hill, London 1983)

[4] D. Burch, 1991. Continuum absorption by H_2O. *Atmospheric Transmission*, Proc. Soc. Photo-Opt. Instr. Eng. 277, 28-39.

[5] S.A. Clough, F.X. Kneizys, and R.W. Davies, 1989. Line Shape and the Water Vapor Continuum. *Atmos. Res.*, **23**, 229-241.

[6] S.A. Clough, M.J. Iacono and J.-L. Moncet, 1992. Line-by-line calculation of atmospheric fluxes and cooling rates: Application to water vapor. *J. Geophys. Res.*, **97**, 15761-15785.

[7] V.I. Formichev and G.M. Shved, 1995. Parameterization of the radiative flux divergence in the 9.6 μm O_3 band. *J. Atmos. Terr. Phys.*, **47**, 1037-1049.

[8] Q. Fu and K.N. Liou, 1992. On the correlated k-distribution method for radiative transfer in nonhomogeneous atmospheres. *J. Atmos. Sci.*, **49**, 2139-2156.

[9] R.R. Gamache, R.L. Hawkins, and L.S. Rothman, 1990. Total Internal Partition Sums in the Temperature Range 70-3000K: Atmospheric Linear Molecules *J. Molec. Spectrosc.*, **142**, 205-219.

[10] R.R. Gamache, and L.S. Rothman, 1992. Extension of the HITRAN Database to Non-LTE Applications. *J. Quant. Spectrosc. Radiat. Transfer*,**48**(5/6), 519-525.

[11] R. Goody, R. West, L. Chen, and D. Crisp, 1989. The Correlated-k Method for Radiation Calculations in Nonhomogeneous Atmospheres. *J. Quant. Spectrosc. Radiat. Transfer*, **42**(6), 539-550.

[12] R.M. Goody and Y.L. Yung: *Atmospheric Radiation : Theoretical Basis, 2nd Edition* (Oxford University Press, New York 1989) 519p.

[13] T.J. Greenwald and G.L. Stephens, 1988. Application of a Doubling-Adding Radiation Model to Visibility Problems. Final Report: March 1988. CIRA, CSU, Ft. Collins, CO, U.S.

[14] M.D. King, W.P. Menzel, P.S. Grant, J.S. Myers, G.T. Arnold, S.E. Platnick, L.E. Gumley, S.-C. Tsay, C.C. Moeller, M. Fitzgerald, K.S. Brown, and F.G. Osterwisch, 1996 Airborne Scanning Spectrometer for Remote Sensing of Cloud, Aerosol, Water Vapor, and Surface Properties, *J. Atmos. Oceanic Technology*, **13**(4), 777-794.

[15] C. Kittel and H. Kroemer: *Thermal Physics* (W.H. Freeman and Co., New York 1980) 473p.

[16] D. P. Kratz, 1995. The Correlated-k Distribution Technique as Applied to the AVHRR Channels. *J. Quant. Spectrosc. Radiat. Transfer*, **53**(5), 501-517.

[17] D. P. Kratz, 1997. The Use of Correlated k-Distribution to Account for the Radiative Effect of Molecular Absorption Upon Satellite Measured Radiances. *9th Conference on Atmospheric Radiation: Preprints* 184-185.

[18] A.A. Lacis and J.E. Hansen, 1974. Parameterization for the Absorption of Solar Radiation in the Earth's Atmosphere. *J. Atmos. Sci.*, **31**, 118-133.

[19] A.A. Lacis, W.C. Wang, and J. Hansen, 1979. Correlated k-distribution method for radiative transfer in climate models: Application to effect of cirrus clouds on climate. In: *Proceedings of the Fourth National Aeronautics and Space Adminstration Weather and Climate Program Science Review* NASA Conf. Publ. 2076, 309-314.

[20] A.A. Lacis and V. Oinas, 1991. A Description of the Correlated k Distribution Method for Modeling Nongray Gaseous Absorption, Thermal Emission, and Multiple Scattering in Vertically Inhomogeneous Atmospheres. *J. Geophys. Res.*, **96**(D5), 9027-9063.

[21] W. Malkmus, 1967. Random Lorentz band model with exponential-tailed S^{-1} line intensity distribution function. *J. Opt. Soc. Amer.*, **57**, 323-329.

[22] R.A. McClatchey, R.W. Fenn, J.E. Shelby, F.E. Volz and J.S. Garing, 1972. *Optical Properties of the Atmosphere* (3rd edition), AFCRL-72-0497, Environmental Research Papers No. 411, Air Force Cambridge Research Laboratory, Bedford, MA, 108pp.

[23] R.A. McClatchey, W.S. Bennedict, S.A. Clough, D.E. Burch, K. Fox, L.S. Rothman, and J.S. Garing, 1973. *AFCRL Atmospheric Absorption Line Parameters Compilation* AFCRL-TR-0096.

[24] National Oceanic and Atmospheric Administration, 1976. *U.S. Standard Atmosphere, 1976.* Washington, D.C., ??pp.

[25] R.E. Roberts, J.E.A. Shelby and L.M. Bibermann, 1976. Infrared Continuum Absorption by Atmospheric Water Vapor in the 8-12 μm Window. *Appl. Opt.*, **15**, 2085-2090.

[26] C. D. Rodgers, 1976. Retrieval of Atmospheric Tempearture and Composition From Remote Measurements of Thermal Radiation. *Rev. Geophysics and Space Physics*, **14**, 609-624.

[27] L.S. Rothman, R.R. Gamache, R.H. Tipping, C.P. Rinsland, M.A.H. Smith, D. Chris Benner, V. Malathy Devi, J.-M. Flaud, C. Camy-Peyret, A. Perrin, A. Goldman, S.T. Massie, L.R. Brown, and R.A. Toth, 1992: The HITRAN Molecular Database Editions of 1991 and 1992. *J. Quant. Spectrosc. Radiat. Transfer*, **48**(5/6), 469-507.

[28] L.S. Rothman, 1996: HAWKS: Hitran Atmospheric Workstation. (CDROM) Laurence S. Rothman, PL/GPOS, 29 Randolph Road, Hanscom AFB, MA 01731-3010.; Ontar Corporation, 9 Village Way, North Andover, MA, 01845.

[29] David S. Saxon: *Elementary Quantum Mechanics* (McGraw-Hill, New York 1968) 426p.

[30] G.L. Stephens: *Remote Sensing of the Lower Atmosphere* (Oxford University Press, New York 1994) 523p.

[31] S.A. Tjemkes and J. Schmetz, 1997. Synthetic satellite radiances using the radiance sampling method. *J. Geophys. Res.*, **102**(D2), 1807-1818.

[32] R.D. West, D. Crisp and L. Chen, 1990. Mapping transformations for broadband atmospheric calculations. *J. Quant. Spectrosc. Radiat. Transfer*, **43**, 191-199.